

CO₂CARE
CO₂ Site Closure Assessment Research

Grant Agreement number:	256625
Project acronym:	CO ₂ CARE
Project title:	CO ₂ Site Closure Assessment Research
Project number:	256625
Call (part) identifier:	FP7-ENERGY-2010-1
Funding scheme:	Collaborative project
Theme:	Energy 2010
Starting date:	01/01/2011
Duration:	36 month

Deliverable

**D3.1 - Review of relevant trapping mechanisms based
on site portfolio**

Due date of deliverable: December 2011
Submitted: December 2011
Dissemination level: PUBLIC

Index of Contents

INDEX OF CONTENTS	2
LIST OF TABLES	2
LIST OF FIGURES	3
1 EXECUTIVE SUMMARY	4
2 Introduction	5
3 Description of storage mechanisms.....	6
3.1 STRATIGRAPHIC AND STRUCTURAL TRAPPING	6
3.2 RESIDUAL TRAPPING	6
3.3 DISSOLUTION TRAPPING.....	10
3.3.1 Diffusion transport.....	11
3.3.2 Convection.....	11
3.3.3 Pressure modification by the dissolution process	12
3.3.4 The effects of numerical dispersion on dissolution simulation	13
3.4 MINERAL TRAPPING.....	16
4 Site specific, long-term trapping analysis.....	19
5 Case studies	22
5.1 REACTIVE TRANSPORT MODELLING OF CO ₂ INJECTION AT SLEIPNER SITE, NORTH SEA	22
5.2 REACTIVE TRANSPORT MODELLING OF CO ₂ INJECTION INTO A METHANE GAS DEPLETED RESERVOIR AT THE K12-B FIELD, NORTH SEA	25
5.3 A PRELIMINARY ASSESSMENT OF THE CONTRIBUTION OF CO ₂ TRAPPING MECHANISMS AT THE KETZIN PILOT SITE.....	27
5.3.1 Assessment of CO ₂ dissolution by reservoir simulations	27
5.3.2 Geochemical model parametrisation.....	28
5.3.3 Geochemical modelling results.....	30
5.3.4 Contribution of trapping mechanisms.....	31
6 References.....	33

List of tables

Table 1: Dissolved amount of CO ₂ as function of grid block size obtained by numerical experiments after injecting 50 million tonne over a 25 year period (Bergmo et al. 2009).....	14
Table 2: Primary minerals introduced into the model based on Förster et al. (2010) and Norden et al. (2010).	28
Table 3: Initial brine composition introduced into the model based on reservoir fluid sample analysis (Förster et al., 2006; Würdemann et al., 2010 and unpublished data).....	29
Table 4: Kinetic rate parameters taken from Palandri and Kharaka (2004), in case of Pyrite from Xu et al. (2010).....	30

List of figures

Figure 1: Conceptual illustration of contribution from the different trapping mechanisms - SRDM – Structural, Residual, Dissolution, Mineral.....	5
Figure 2: Examples of (a) structural and (b) stratigraphic physical traps for CO ₂	6
Figure 3: The snap-off process creating residual trapped gas during imbibition when brine returns to the CO ₂ filled medium.	7
Figure 4: Relative permeability curve for macroscopic behaviour with hysteresis.....	7
Figure 5: Relative permeability curve for macroscopic behaviour with hysteresis, taken from Oak (1990) for a water wet Berea sandstone.	8
Figure 6: Database of trapping capacity $\phi S(nw)r$ versus initial non-wetting phase saturation $S(nw)_i$ in the literature. The higher initial saturation, the more potential for residual trapping.	9
Figure 7: Large-scale effect of residual trapping after injection stop (Juanes et al. 2006)...	9
Figure 8: Comparison between density-driven convection in the modelled system (left) and experimental system (right).	12
Figure 9: Predicted apparent molar volumes of CO ₂ in water compared with experimental results.	13
Figure 10: Fraction of CO ₂ dissolved as function of the relative grid block size.....	14
Figure 11: Variation of CO ₂ solubility in water with salinity, for various conditions representative of sedimentary basins.	15
Figure 12: Temporal variation of resistivity in the observation well OB-2. The colour scale shows differential value from baseline data.	16
Figure 13: Classification of characteristic minerals of siliciclastic CO ₂ storage formations according to their reaction kinetic and properties.	17
Figure 14: A) Diagram showing the concept of increasing amount of immobile CO ₂ , and thereby increased security of the storage facility.	19
Figure 15: Output diagram from the TOUGHREACT simulation of the base-case by Zhang et al. 2009, forming the basis for the re-calculated proportions.	20
Figure 16: Illustration of the different elements in the trapping of CO ₂	21
Figure 17: Dense phase saturation SG (top) and mass fraction of dissolved CO ₂ in the pore water XCO ₂ L (bottom), after 25 years of injection.	23
Figure 18: Dense phase CO ₂ saturation (SG) and mass fraction of dissolved CO ₂ in the pore water (XCO ₂ L) simulated 50, 1000, 2000, 5000 and 10000 years after injection.	24
Figure 19: Evolution of calcite, albite, chlorite and dawsonite mineral contents in the Utsira formation, 10000 years after CO ₂ injection.....	25



Figure 20: Distribution of the pH values in the reservoir and the first cap-rock after 10 years of CO ₂ injection, allowing the distinction of four different zones.	26
Figure 21: Spatial distribution of the CO ₂ plume at the Ketzin site in 2300 under the assumption of 70,000 t CO ₂ being injected until the end of April 2013.	27
Figure 22: Spatial distribution of dense phase (left) and dissolved CO ₂ (right) at the Ketzin pilot site in 2300.	28
Figure 23: Changes in mineral volumes resulting from geochemical simulations, in cm ³ /m ³ of rock.	31
Figure 24: Contribution of the four CO ₂ trapping mechanisms, whereas the residual trapped CO ₂ ratio is included in the gas phase (structural trapped CO ₂) and the mineralized CO ₂ ratio in the dissolved CO ₂ (structural trapped and dissolved CO ₂ sum up to 100%). ...	32

1 Executive Summary

This deliverable describes the chemical/physical background for the mechanisms for long-term stabilisation and immobilisation of CO₂. Based on this it is suggested how to evaluate the quantitative contribution from each mechanism to the trapping over time. The suite of mechanisms is also termed “SRDM” for **S**tructural and stratigraphic trapping, **R**esidual trapping, **D**issolution in the brine, and **M**ineral trapping by geochemical fluid/mineral reactions and precipitation of minerals.

The quantitative contribution of each of these trapping mechanisms will be site-dependent, as the combination of the injection strategy, geological architecture and the migration pattern at later stages of stabilisation will determine their efficiency in immobilising parts of the CO₂ plume. This is illustrated by case studies from different storage sites.

2 Introduction

The mechanisms for long-term stabilisation and immobilisation of CO₂ are:

1. Structural and stratigraphic trapping,
2. Residual trapping,
3. Dissolution in the brine (+dissolution enhancement by induced convection), and
4. Mineral trapping by geochemical fluid/mineral reactions and precipitation of minerals.

The quantitative contribution of each of these trapping mechanisms will be site-dependent, as the combination of the injection strategy, geological architecture and the migration pattern at later stages of stabilisation will determine their efficiency in immobilising parts of the CO₂ plume.

The overall aim of this activity is to be able to describe the relative contribution and the combined effect of these different trapping mechanisms for one or more selected sites by applying modelling tools combining thermo-hydraulic and geochemical processes. The ultimate goal is to be able to supply input data for a site-specific “Trapping-Safety-Time” plot. So far only the very conceptual plot from the IPCC report is widely used to illustrate the long-term safety development for geological storage (Fig. 1).

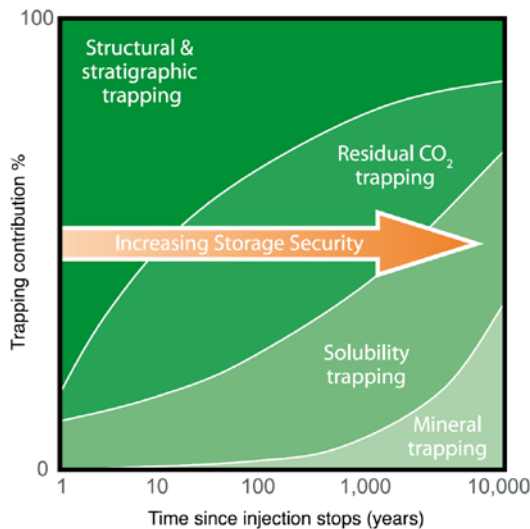


Figure 1: Conceptual illustration of contribution from the different trapping mechanisms - SRDM – Structural, Residual, Dissolution, Mineral. (From Benson, S.M. and Cook, P.J., 2005).

Calibration of modelling examples will possibly be carried out using monitoring data from the sites where aspects of the trapping processes have already been described in earlier research and where suitable data might be available (Frio, Nagaoka, Otway, Sleipner and Ketzin).

The present site portfolio includes Ketzin, K12-B, Sleipner and Otway, each representing very different (hydro) geological and environmental settings (i.e. natural gas reservoir / saline aquifer), and each of these poses different challenges concerning modelling of storage mechanisms.

3 Description of storage mechanisms

3.1 Stratigraphic and structural trapping

Initially, physical trapping of CO₂ below low-permeability seals (caprocks), such as very-low-permeability shale or salt beds, is the principal means to store CO₂ in geological formations. Sedimentary basins have such closed, physically bound traps or structures, which are occupied mainly by saline water, oil and gas. Structural traps include those formed by folded or fractured rocks. Faults can act as permeability barriers in some circumstances and as preferential pathways for fluid flow in other circumstances. Stratigraphic traps are formed by lateral changes in rock type caused by variation in the setting where the rocks were deposited. Both of these types of traps are suitable for CO₂ storage.

A special case for structural trapping can occur in saline formations that do not have a closed trap but consists of a slightly tilted aquifer where fluids migrate very slowly over long distances. When CO₂ is injected into a formation, it displaces saline formation water and then migrates buoyantly upwards, because it is less dense than the water. When it reaches the top of the storage formation, it continues to migrate as a separate phase until it is dissolved (potentially helped by gravity instability and mixing), trapped as residual CO₂ saturation or gets arrested in local structural or stratigraphic traps below the sealing formation (IPCC 2005).

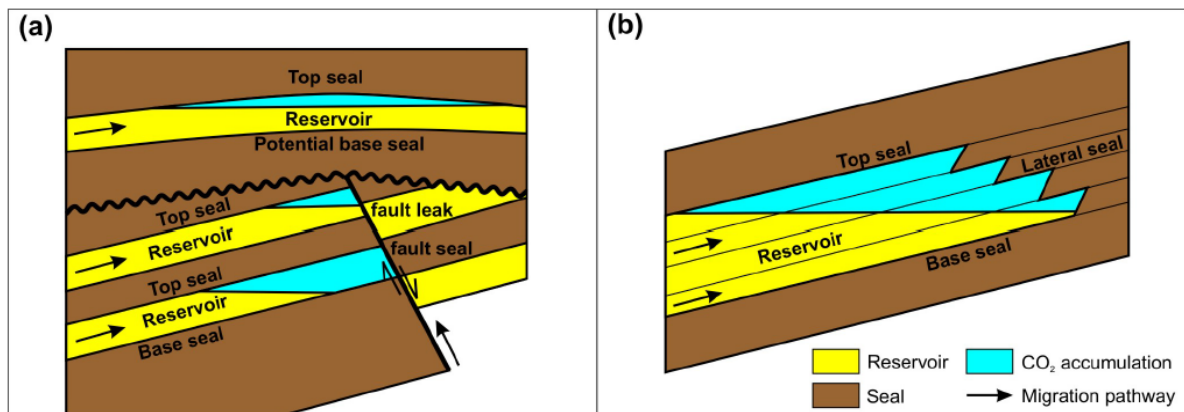


Figure 2: Examples of (a) structural and (b) stratigraphic physical traps for CO₂ (From CO2CRC, 2008).

3.2 Residual trapping

Consider a medium that is initially filled with water or brine. The solid grains are usually made of minerals that are naturally wetting to water and, therefore the medium is preferentially water wet. During CO₂ injection into the aquifer or reservoir, the nonwetting CO₂ phase invades the pore space. This is a drainage process in which the only mechanism for displacement of water by CO₂ is piston-type displacement: the CO₂ invades the porous medium in the form of a continuous, connected cluster. Water, however, remains present not only in small pores that have not been filled with CO₂ but also in the corners and crevices of the pores that have been invaded. Consider now the displacement

of the CO₂ by water. During this process, there are several physical mechanisms by which the water can displace the CO₂ (Lenormand et al., 1983). In addition to piston-type displacement, cooperative pore-body filling and snap-off may occur (Fig. 3). For water wet rocks, snap-off is the dominant mechanism (Al-Futaisi and Patzek, 2003; Valvatne and Blunt, 2004). The important point is that snap-off and cooperative filling may lead to disconnection and bypassing of the CO₂ (Juanes et al. 2006).

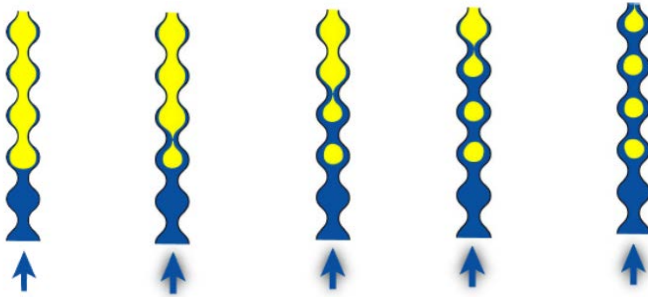


Figure 3: The snap-off process creating residual trapped gas during imbibition when water or brine returns to the CO₂ filled medium (Tchelepi 2009).

The macroscopic consequences of these porescale processes are trapping and relative permeability hysteresis. In accordance with the pore-scale explanation give above, experimental data strongly suggest that the nonwetting phase experiences much more pronounced hysteresis than the wetting phase (Juanes et al. 2006).

Residual Trapping of the non-wetting phase (CO₂) is caused by wettability and capillary effects in porous media. The treatment of trapping in this paper follows the hysteresis model of Land (1968). Figure 4 shows the relative permeability curves for CO₂ injection. During injection, when the CO₂ phase (dense phase) saturation increases, the relative permeability curve for CO₂ follows the drainage relative permeability curve $k_{rg}(d)$ (black curve). If at a saturation S_{gi} , the saturation decreases, the relative permeability curve for CO₂ would follow the imbibition curve $k_{rg}(i)$ (red curve). If the saturation continues to decrease until k_{rg} is zero, the residual trapped non-wetting-phase saturation S_{gt} is reached. In Figure 4, $S_{g,max}$ is the maximum saturation and $S_{gt,max}$ is the maximum trapped saturation. Spiteri et al. (2005) provide a summary of other residual trapping models (Nghiem et al. 2009).

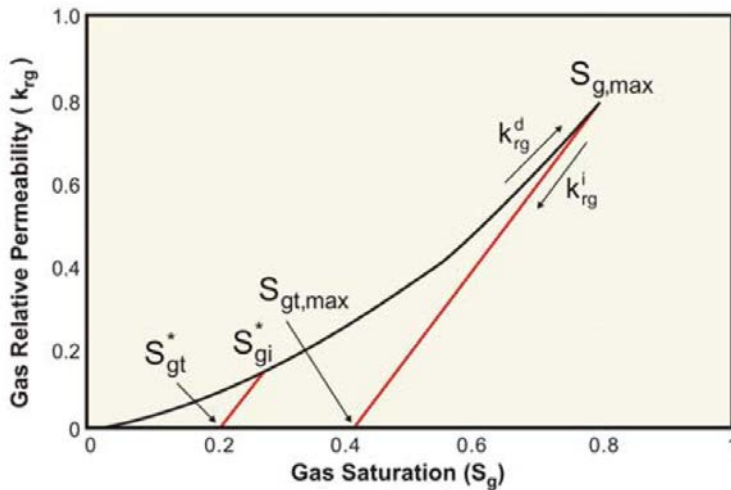


Figure 4: Relative permeability curve for macroscopic behaviour with hysteresis (Nghiem et al. 2009).

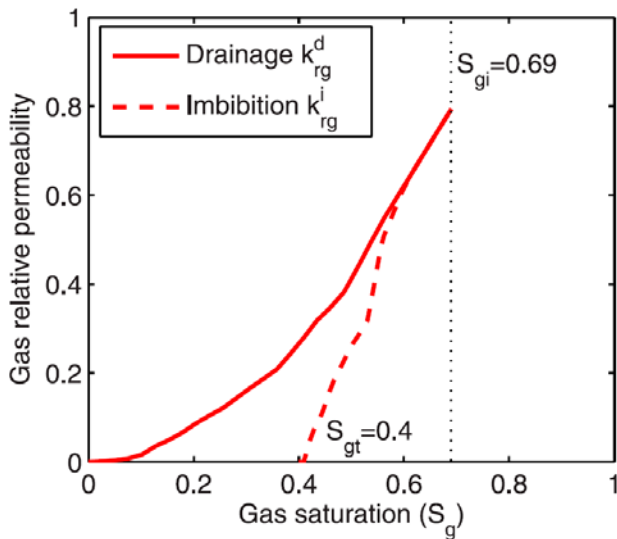


Figure 5: Relative permeability curve for macroscopic behaviour with hysteresis, taken from Oak (1990) for a water wet Berea sandstone (Juanes et al. 2006).

In many sedimentary rocks, supercritical CO₂ is typically the non-wetting phase relative to the ambient brine. At the front of the CO₂ plume, the CO₂ saturation increases, and the brine is drained from the pore space. The capillary entry pressure prevents the drainage of the brine from the smallest pores, resulting in an incomplete displacement. We refer to the brine left behind the advancing CO₂ front as the residual brine S_{br} . Bachu & Bennion (2007) showed with laboratory experiments that S_{br} can range from 0.2 to 0.68 at storage conditions in saline aquifers. The high end of these values is surprising and may in part be due to heterogeneity and gravity segregation in the experiments. They also show that the presence of residual water reduces the apparent permeability of the CO₂ to approximately 1/5 of the single-phase permeability. We refer to this value as the relative permeability of CO₂, denoted k_{rc} . If the CO₂ plume is migrating laterally as a gravity current, the CO₂ saturation decreases at the trailing edge of the plume (Figure 7), and the ambient brine imbibes into the pore space previously occupied by CO₂. Preferential imbibition of the brine into the smaller pores and interfacial instabilities leave CO₂ behind as disconnected

bubbles and ganglia of CO₂ which are effectively immobile. We refer to this immobile CO₂ saturation as the residual CO₂ saturation, S_{cr} , and to the process as residual trapping. Bachu & Bennion (2007) report values of S_{cr} from 0.1 to 0.35 for saline aquifers in the Alberta basin, indicating that they will trap CO₂ efficiently. Most work on residual trapping during CO₂ storage has focused on the effect of hysteresis on the magnitude of S_{cr} , and the design of injection strategies that maximize residual trapping during, or shortly after, the injection period (Mo et al. 2005; Juanes et al. 2006; Ide, Jessen & Orr 2007, Hesse et al. 2008).

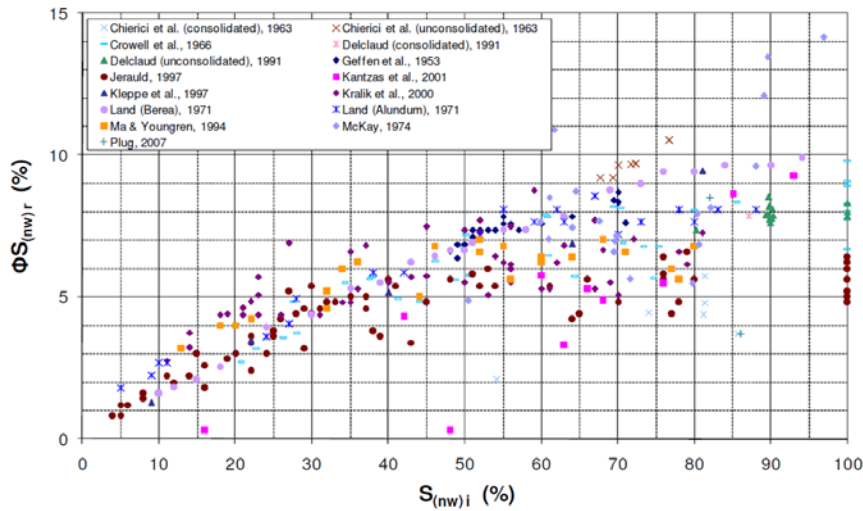


Figure 6: Database of trapping capacity $\phi S_{(nw)r}$ versus initial non-wetting phase saturation $S_{(nw)i}$ in the literature. The higher initial saturation, the more potential for residual trapping (Mansoori et al. 2009).

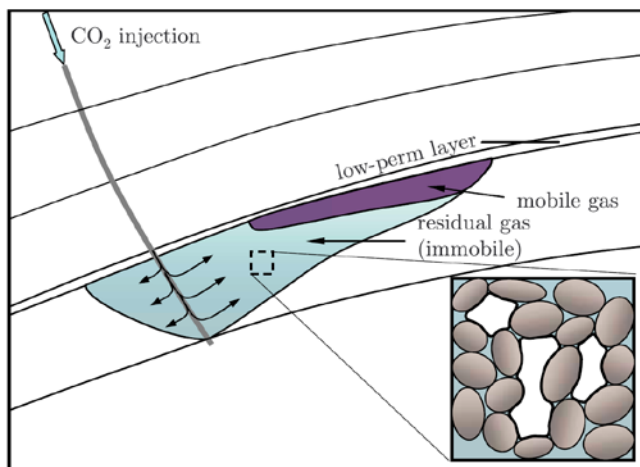


Figure 7: Large-scale effect of residual trapping after injection stop (Juanes et al. 2006).

Results suggest that lateral migration of the injected CO₂ along the seal will trap the CO₂ relatively quickly as residual saturation. Residual trapping is quite effective in sloping aquifers with small mobility ratios and high residual CO₂ saturations (Hesse et al. 2008).

Injection of water slugs alternating CO₂ injection (in the spirit of classical WAG for enhanced oil recovery (Spiteri and Juanes, 2006) increases the effectiveness of the

storage project. The injected water forces breakup of large connected CO₂ plumes, enhancing trapping and immobilization of the CO₂. On the other hand, a WAG strategy leads to higher bottom hole pressures at injection wells, which may be limited by seal integrity, regulatory or economical constraints. The identification of WAG as a potentially effective strategy for CO₂ storage lends itself to an optimization problem to maximize the amount of trapped CO₂ by varying the well rates and well completions, subject to BHP constraints. The hysteresis effect is also in action when injection is stopped intermittently for well maintenance or other activities.

Coarse simulation models will overestimate the sweep and subsequent capillary trapping of CO₂. An accurate assessment of the different storage mechanisms (hydrodynamic, capillary, solution and mineral trapping) requires high-resolution models that capture the migration paths of the injected CO₂ in the subsurface (Juanes et al. 2006).

Most papers dealing with residual gas trapping have focussed on the process during the natural equilibration of the CO₂ plume after injection stop. However, from our safety perspective and to derive the amount of residual trapping that will immobilise CO₂ in the total system at a given time-step, the quantification of the residual part must include the amount that is left behind if we tried to empty the structure for mobile gas ultimately by drilling wells (leaks) into the gas cap.

3.3 Dissolution trapping

When CO₂ dissolves in formation water, a process commonly called solubility trapping occurs. The primary benefit of solubility trapping is that once CO₂ is dissolved, it no longer exists as a separate phase, thereby eliminating the buoyant forces that drive it upwards. The CO₂ solubility in formation water decreases as temperature and salinity increase. Dissolution is rapid when formation water and CO₂ share the same pore space, but dissolution outside the immediate contact zone is slow since it depends on diffusion as the transport mechanism. Over longer time-spans, the increased density of the brine with dissolved CO₂ can create gravitational instability and may cause convection that mixes the different brines and further enhances dissolution.

The significance of the dissolution trapping, the quantitative proportion, and the influence on pressure increase have been reviewed and discussed by Thibeau et al. (2011), stating slight warnings about the limitations in the capacity enhancing effects of these interactions. These views are cited below.

As underlined by various authors (Bachu et al. 2007), CO₂ dissolution is a significant trapping mechanism and saturating formation water with CO₂ would create huge CO₂ storage capacities (Bachu & Adams, 2003). Nevertheless, it is also indicated that dissolving CO₂ is a long-term process, coupling molecular diffusion and in some cases aided by gravitational instabilities in the formation water.

- On the Utsira case, dissolution processes is expected to develop from 300 to 5000 years after the injection period (Chadwick et al. 2008),
- a 1000 year period is modelled to dissolve the CO₂ by Van der Meer & Wees (2006),
- a parametric study is presented by Ennis-King & Paterson (2003) illustrating the impact of the permeability anisotropy on the time required to dissolve the CO₂, with 25% of the CO₂ being dissolved after 300 to 20000 years depending on the kv/kh ratio.

As such, CO₂ is expected to significantly dissolve a long time after the end of the injection period. For an industrial storage project, the question is then how much CO₂ can reasonably dissolve during the injection period, which could reduce the pressure pulse due to the CO₂ injection? Simple assumptions are made to evaluate the fraction of CO₂ that can dissolve during the injection period. Indeed, CO₂ injection results in drainage processes only, no imbibition is to take place before injection stops; CO₂ dissolves into formation water in direct contact with the CO₂ dense phase, and molecular diffusion (transportation of dissolved CO₂) can be neglected due to the short time-span in question; the formation water in direct contact with CO₂ in dense phase is the residual water in CO₂ flooded areas. With typical numbers of 20% residual water saturation, a CO₂ content of the CO₂ saturated aqueous phase of 50 kg/m³ and a CO₂ density of 500 kg/m³, one gets:

- dissolved CO₂ mass per unit of pore volume of: 20% × 50 = 10 kg/m³;
- dense phase CO₂ mass per unit of pore volume of: 80% × 500 = 400 kg/m³.

Hence, less than 3% of the CO₂ is to dissolve in the formation water. As a consequence of these, a very limited fraction of CO₂ is expected to dissolve in the formation water during the injection period and this dissolution is expected to have a minor impact when it comes to pressure build up due to CO₂ injection (Thibeau et al. 2011).

3.3.1 Diffusion transport

Diffusion will transport CO₂ away from the interface between aqueous and gas phases, thus providing a mechanism for dissolving additional CO₂, although as a very slow process. The rate of transport has been illustrated with a calculation by Pruess and Nordbotten (2011). The diffusivity of CO₂ is approximately $D = 2 \times 10^{-9} \text{ m}^2/\text{s}$ (Tewes and Boury 2005; Farajzadeh 2009); which leads to an effective diffusivity of $D_{\text{eff}} = 1 \times 10^{-9} \text{ m}^2/\text{s}$. After 300 years ($= 9.5 \times 10^9 \text{ s}$) it would penetrate a distance of only 3.1m into the aqueous phase, which is equal to a movement of approximately 1 cm/year. The process has therefore absolutely no distribution effect during the injection period. In the longer time-scale after injection has stopped, the main interest in the diffusion transport mechanism should be linked to the caprock

3.3.2 Convection

A recent review of the processes involved in density-driven brine convection has been presented by Kneafsey and Pruess (2011), and is quoted in the following. At some distance from the injection well where the CO₂ has spread out under the cap rock, there will likely be a nearly horizontal interface between a free CO₂ phase above and the aqueous phase below. Geometric details of the interface will be affected by the properties of the porous media; for simplicity, we will consider the interface to be flat. At the interface, CO₂ will dissolve into the aqueous phase. If the aqueous phase was immobile, the rate of CO₂ dissolution would be limited by the rate at which CO₂ can be removed from the interface by molecular diffusion. This is a slow process, and the rate of CO₂ dissolution will decrease with time. CO₂ dissolution causes the density of the aqueous phase to increase on the order of 0.1 to 1%, depending on CO₂ pressure, temperature, and salinity (Garcia 2001). This density increase induces a gravitational instability because denser CO₂-rich aqueous fluid overlies less-dense fluid. The instability can trigger convection of fluid at a variety of scales, which could greatly increase the rate at which dissolved CO₂ is removed from the interface with the overlying free CO₂, thereby accelerating CO₂ dissolution. CO₂ dissolution-induced convection has been studied by many investigators because of its

relevance for security and permanence of CO₂ storage. The earliest published study on CO₂ dissolution-induced density increase and its importance for CO₂ storage was by Weir et al. (1995, 1996). Lindeberg and Wessel-Berg (1997) evaluated the conditions under which vertical convective flow will occur in a medium subjected to both a thermal gradient and the presence of a CO₂ dissolution-induced dense layer. Lindeberg and Bergmo (2003) examined multiscale numerical simulation problems related to the Sleipner Vest CO₂ storage project in the Norwegian Sector of the North Sea. Studies have also been performed investigating stability analysis for the onset time for convection, the preferred wavelength for the growth of convective fingers, and growth rates (e.g., Ennis-King and Paterson 2003a,b; Ennis-King et al. 2005; Hesse et al. 2006; Riaz et al. 2006; Xu et al. 2006). This summary by Kneafsey and Pruess (2010) is associated with analysis and comparison of laboratory flow experiments and modelling of these systems with a numerical model using TOUGH2 and they found good agreement (Figure 8).

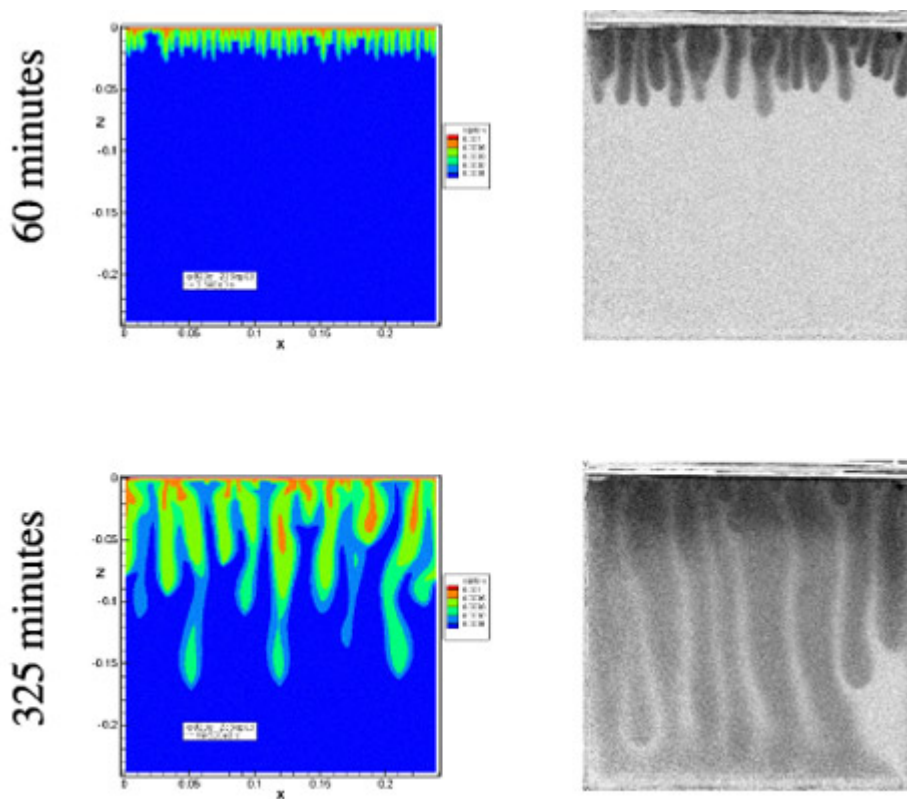


Figure 8: Comparison between density-driven convection in the modelled system (left) and experimental system (right) (From Kneafsey and Pruess (2010)).

3.3.3 Pressure modification by the dissolution process

Moreover, as indicated in Ennis-King & Paterson (2003), the apparent partial molar volume of dissolved CO₂ is in the range of 30-40 cm³ in geological storage conditions, to be compared with 88 cm³ for a 500 kg/m³ dense phase CO₂. So, even if all the injected CO₂ dissolves in the water, it would take as much space as a dense phase CO₂ with a density from 1100 to 1500 kg/m³, leading to similar pressure build up issues in the aquifer (Thibeau et al. 2011).

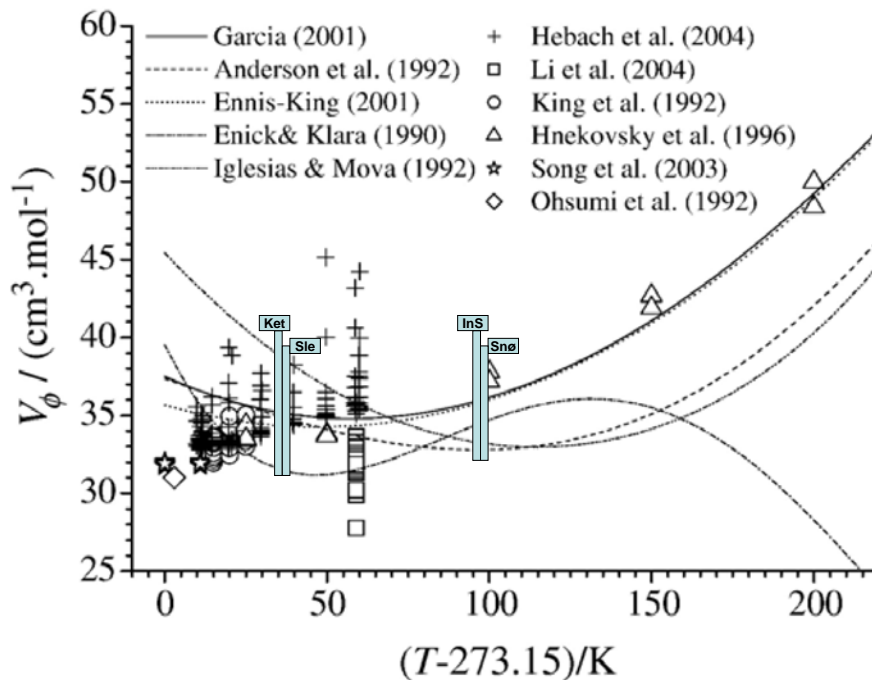


Figure 9: Predicted apparent molar volumes of CO₂ in water compared with experimental results. The apparent molar volume model of Ennis-King (2001) was given by Garcia (2001) through his personal communication with Jonathan Ennis-King. The apparent molar volumes of Hnekovsky et al. (1996) are directly given by the original authors. The other apparent molar volumes are calculated with experimental densities, where the water densities are calculated with Eq. (2). The CO₂ solubilities corresponding to the saturated density data of Li et al. (2004) and Hebach et al. (2004) are calculated with the model of Duan et al. (2006) (Figure from Hu et al. 2007). Selected sites posted on the figure.

3.3.4 The effects of numerical dispersion on dissolution simulation

The background for a typical error occurring in standard numerical simulations of CO₂ storage including flow and dissolution processes has been reviewed by Bergmo et al (2009) and by Pickup et al. (2010). Bergmo et al (2009) devised an extrapolation method to describe the effect of numerical dispersion, which is reproduced in the following. It should be noted that numerical dispersion and the error induced will be dependent on the numerical scheme. The example quoted here is a selected example for only one numerical implementation.

The dissolution of CO₂ is governed by diffusion and consequently by how much brine is contacted by the CO₂. In numerical modelling the amount of dissolved CO₂ will be exaggerated due to numerical dispersion. When a new grid block is contacted by CO₂ in the front of a migrating plume all the brine in the grid block has to be saturated with CO₂ before any free CO₂ will appear. This error will be larger for larger grid blocks. To estimate this error a series of simulations on the detailed model with a systematic variation of grid block sizes has been performed. The results show that the numerical error exaggerates the dissolution with more than 100 % on the short term (during the injection period) when using 500 m grid blocks compared to the limiting case with infinitely small grid blocks. On

the long term the error gradually decreases. The results also show that the resolution does not have a pronounced effect of the distribution of CO₂. The diameter of the plume is approximately 7 km for the finest grid and approximately 1 km larger for the coarsest grid. Only the lateral resolution of the grid was changed because the distribution of CO₂ is mainly dominated by the gravity driven lateral migration under the cap rock both in the injection period and on long-term scale. The simulated amount of dissolved CO₂ for each of the five cases is given in Table 1.

The dissolutions were fitted to a power function of the grid block size and the results are plotted in Figure 9. If this function is extrapolated to zero grid block size an upper bound for the dissolved amount of CO₂ is estimated to 4.6 %. This is an empirical approach and the theoretical justification to extrapolate the curve to zero has not yet been performed. This estimate is valid only for the injection period. (Bergmo et al 2009).

The calculation of pressure modification by dissolution of CO₂ performed above by Thibeau et al (2011) in combination with the estimate of the amount of dissolved CO₂ for the Sleipner case by Bergmo et al. (2009) indicates that the 4.6% dissolved CO₂ only takes care of approximately 5-6% of the volume that causes the pressure increase, and therefore is a small contribution to mitigating overpressure.

The background calculation is that for each mole CO₂ that dissolves, 88 cm³ disappears, but water enlarges with 30-40 cm³. So net volume reduction is 48-58 cm³ corresponding to 55-66% volume reduction. If in total reservoir 4.6% mass dissolves (as in Bergmo et al. 2009) then 9.2% volume is dissolved (CO₂ density ~½ of brine), and 55-66% of the 9.2% is = 5-6% volume reduction.

Table 1: Dissolved amount of CO₂ as function of grid block size obtained by numerical experiments after injecting 50 million tonne over a 25 year period. (Bergmo et al 2009).

Gird block side length, m	Relative grid block size	Fraction of CO ₂ dissolved
25	1	0.049
50	4	0.054
100	16	0.060
200	64	0.070
500	400	0.103

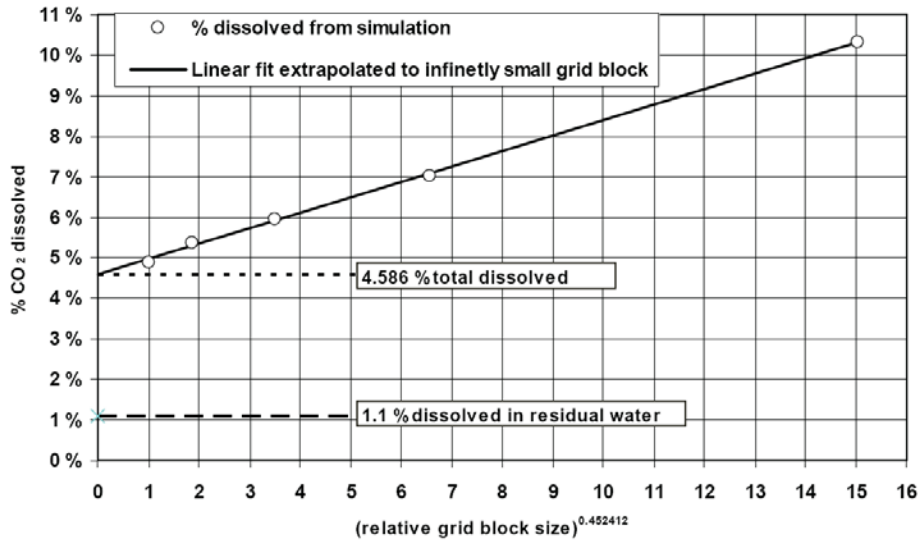


Figure 10: Fraction of CO₂ dissolved as function of the relative grid block size. The dependence has been extrapolated to a grid block size equal to zero corresponding to an infinite number of grid blocks (Bergmo et al 2009).

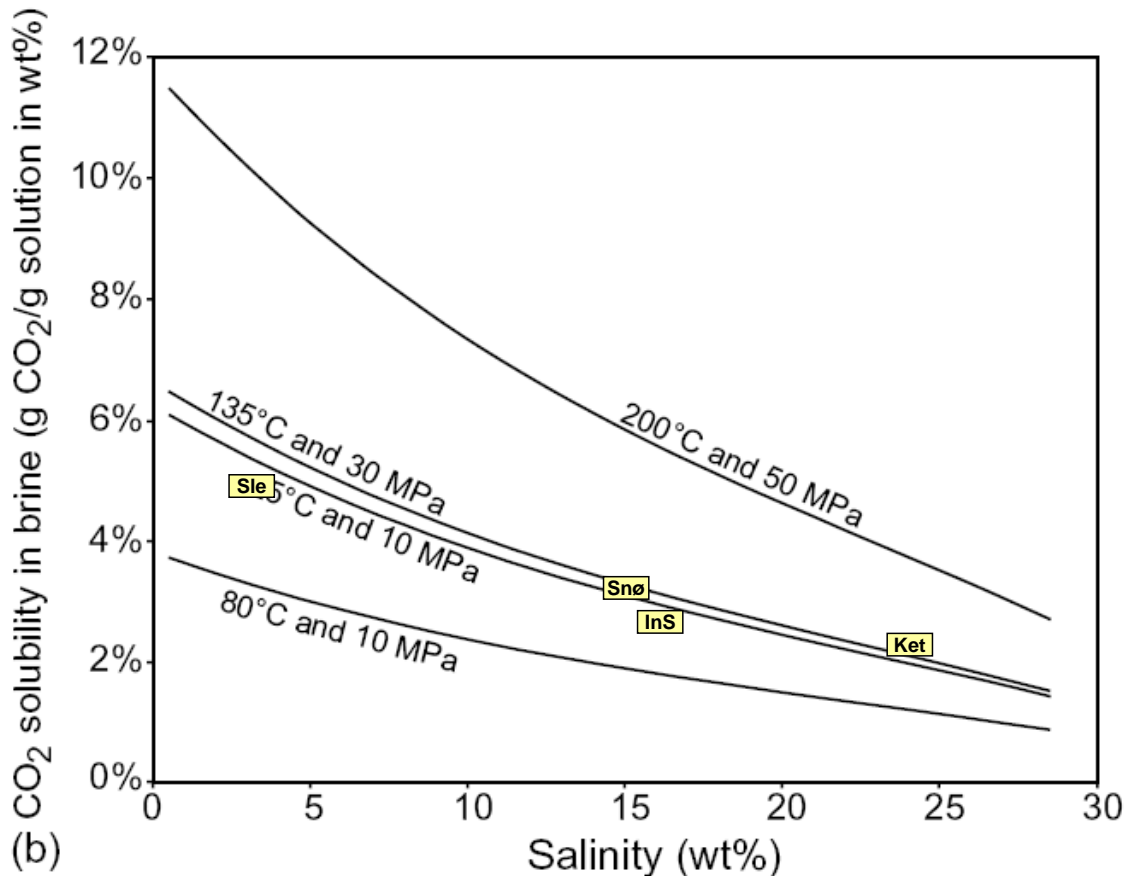


Figure 11: Variation of CO₂ solubility in water with salinity, for various conditions representative of sedimentary basins (Bachu & Adams, 2003). Selected sites posted.

An interesting option could be to obtain data from injection sites where the amount of dissolved CO₂ is quantified. This could then serve as matching data for simulation of the physical process and act as verification set. One example where time-lapse data exist for dissolved CO₂ is the Nagaoka site (from Sato et al. 2011).

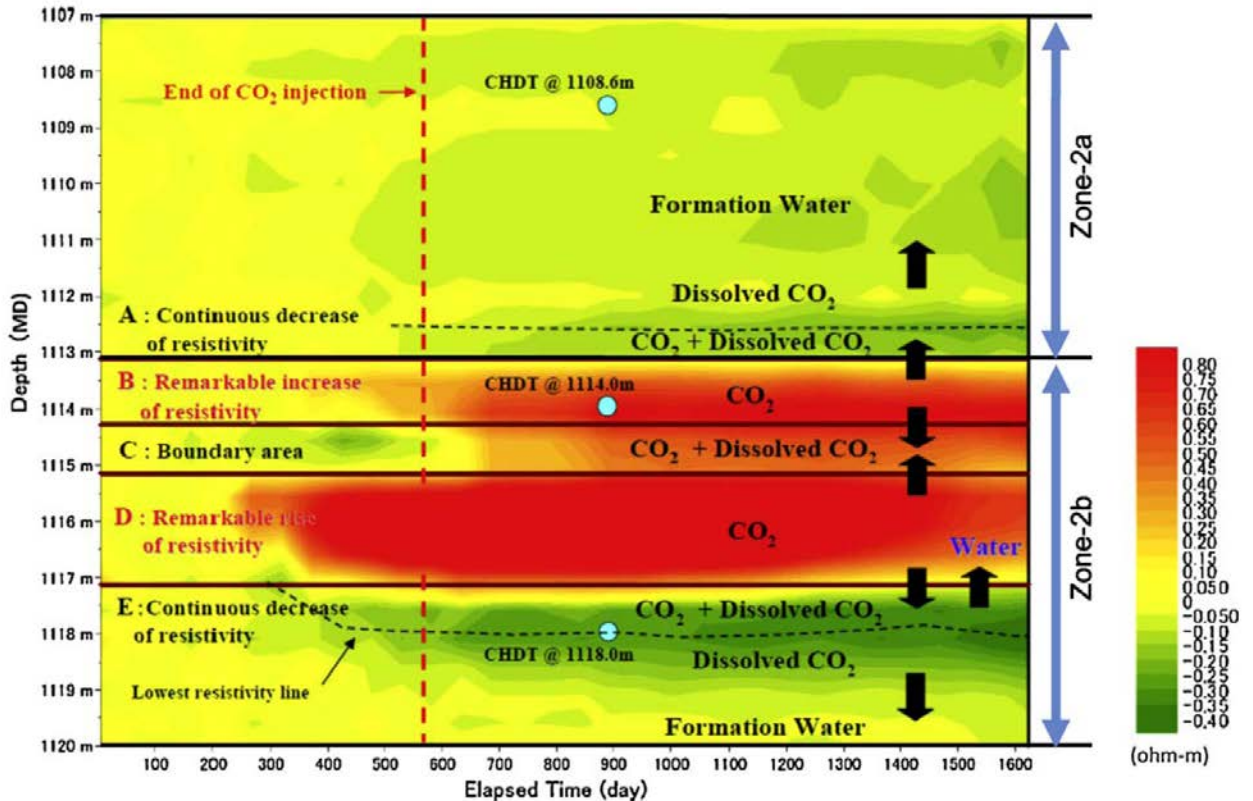


Figure 12: Temporal variation of resistivity in the observation well OB-2. The colour scale shows differential value from baseline data (From Sato et al. 2011).

3.4 Mineral trapping

One of the criteria that have to be fulfilled when assessing the impact of CO₂ storage is the evolution of the storage site towards a situation of long-term stability. Mineral trapping is a time dependent process whose contribution to CO₂ immobilisation increases slowly with time, representing CO₂ incorporated into minerals due to chemical precipitation (Gaus et al., 2008). While during injection phase mineral trapping is almost negligible (Bachu et al., 2007), it constitutes a safe mechanism with a large storage potential when considering residence times in the order of geologic times (Audigane et al., 2007).

It has to be stressed out that the presence of a water phase is essential to chemical reactions; dry gas and rock interactions are orders of magnitude slower and less relevant than those occurring in aqueous solutions, and are usually neglected. Depleted gas reservoirs with low residual water saturation are therefore less prone to chemical alteration due to CO₂ injection. Once the CO₂ is in the subsurface, geochemical interactions within the fluid as well as between the fluid and the rock matrix will take place. First CO₂ dissolves in the formation fluid, acidifying it (see dissolution trapping). This will lead to fast

dissociation of carbonic acid to form the bicarbonate ion. Primary host rock minerals will start to dissolve due to low pH, releasing divalent cations which react with the dissolved bicarbonate species forming Ca, Mg and Fe (II) carbonates. If carbonate and sulfate minerals are being solved from the matrix to buffer the pH, the reaction kinetic will be fast. This will especially be the case during injection phase in the near well environment. In the time after injection, however, slow reactions, which play the major role in terms of mineral trapping, will continue to take place. Aluminosilicate minerals such as clay minerals, micas, chlorites and feldspars that can function as cation donors dissolve very slow at reservoir temperatures. Since precipitation of carbonate minerals requires Ca and Mg sources, siliciclastic formations are considered more suitable for CO₂ storage than carbonate formations which are fast pH buffer (Zhang et al., 2009). In addition to fast and slow dissolution/precipitation kinetic reactions, other aqueous reactions like redox processes, sorption and ion exchange could play a role. Figure 13 classifies minerals that are characteristic of siliciclastic CO₂ storage formations according to their reaction kinetic and properties.

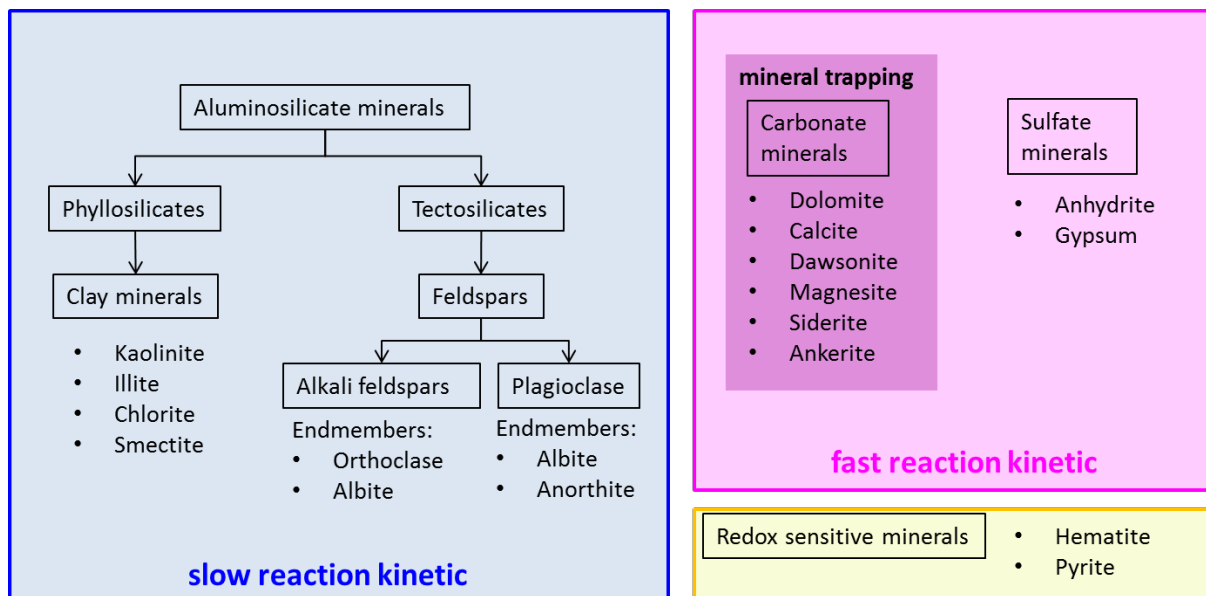


Figure 13: Classification of characteristic minerals of siliciclastic CO₂ storage formations according to their reaction kinetics and properties.

Factors that affect rate and capacity of mineral trapping are the chemical composition of formation waters and of the rock matrix (primary minerals), initial CO₂ fugacity, temperature and pressure as well as dissolution and precipitation kinetic rates (Zerai et al., 2006). Kinetic rate law depends among other parameters on reactive surface area which is very difficult to estimate. Pressure, temperature and also the salinity of the fluid have an impact on CO₂ properties, such as density, viscosity and solubility. Therefore arises the question: How should long-term mineral trapping capacity be assessed? Considering the complexity and interdependency of chemical and physical processes as well as the time factor, numerical modeling turns out to be the best tool to use, backed up where possible by laboratory experiments (Soong et al., 2004; Labus & Bujok, 2011). Site specific long-term geochemical or reactive transport modeling results show that for CO₂ disposal in deep saline siliciclastic aquifers, mineral trapping will occur primarily in the form of dawsonite (NaAlCO₃(OH)₂) and the calcite-group carbonates, most significantly siderite

(FeCO_3), ankerite ($\text{Ca}(\text{Fe}, \text{Mg}, \text{Mn})(\text{CO}_3)_2$), magnesite (MgCO_3), calcite (CaCO_3) and their solid solutions (Gaus et al., 2005; Xu et al., 2010; Johnson et al., 2004; Zerai et al., 2006; Zhang et al., 2009). In favorable cases mineral trapping capacity would be comparable to that of solubility trapping reaching up to 7-10 kg per m^3 medium (Xu et al., 2004; Xu et al., 2010; Zhang et al., 2009). An often-cited reaction is the alteration of albite resulting in permanent trapping of CO_2 as dawsonite (Audigane et al., 2007; Gaus, 2010; Labus & Bujok, 2011; Gaus et al., 2005; Zerai et al., 2006):

$$\text{NaAlSi}_3\text{O}_8 + \text{CO}_2 + \text{H}_2\text{O} \leftrightarrow \text{NaAlCO}_3(\text{OH})_2 + 3\text{SiO}_2$$

albite
dawsonite
chalcedony

The detailed level of knowledge and data needed for the modeling is joined by uncertainties, especially with regard to kinetic of long-term reactions. Estimation of reactive surface area may be based on geometric surface area (Gaus et al., 2005; Xu et al., 2010; Cantucci et al., 2009), therefore different approaches are available. Once this is done and since mineral surface is not smooth, a surface roughness factor could be defined, increasing geometric-based surface value. If it is taken into account that only selective sites of the mineral surface are involved in the reaction, geometric-based surface value could be decreased up to three orders of magnitude. Not all authors consider all of these effects, but they all seem to agree on the fact that reactive surface area for precipitating minerals is very difficult to estimate, thus same values of dissolution are mostly used for precipitation. Gaus et al. (2005) solves the problem by assuming that 50% of total reactive surface area corresponds to the surface area for precipitating minerals. Since the quantification process is questionable and its impact on results could be of several orders of magnitude (Zerai et al., 2006), uncertainty in reactive surface area is often assessed through sensitivity analysis (Gaus et al., 2005; Zhang et al., 2009). Difficulties concerning consistency in thermodynamic databases (differences in equilibrium constants used in the internal database of numerical codes) and activity models at high salinity of the formation fluid also affect the reliability of modeling results (Gundogan et al., 2010).

Besides increasing the accuracy of input data and working on availability of unknown parameters, derivation of consolidated findings from CO_2 -analogues constitutes a further challenge. Natural CO_2 -rich reservoirs (analogues) are widespread: Montmiral (Southeast Basin, France), Messokampos (Florina Basin, Greece), Triassic Lam Formation (Shabwa Basin, Yemen), Honggang Anticline (Songliao Basin, China) are some of them. It is expected that they could reveal which CO_2 trapping minerals actually may form. There are doubts about dawsonite being able to trap CO_2 permanently. It has been suggested that it becomes unstable as reservoir pressure decreases after injection (Hellevang et al., 2005). Also the difficulty to verify dawsonite formation through laboratory experiments supports the skepticism. On the other hand it has been found in many CO_2 analogues (Worden, 2006; Liu et al., 2011), providing evidence of its existence in connection with high CO_2 pressure. This highlights the fact that mineral trapping relies on time-scale. Since analogues act as long-term laboratories it is crucial to incorporate them into the analysis. Information about geochemical interaction and their impact on reservoir lithologies, the existence of a flow regime and the thermodynamic equilibrium conditions vs. time could also be deduced from the studies of natural analogues (Gaus et al., 2005 (2)).

4 Site specific, long-term trapping analysis

The very common illustration of the trapping mechanisms and the storage safety development over long time perspectives is the trapping mechanism/safety plot as published in the Chapter 5 of the IPCC report (IPCC 2005), see figure 14. This generic diagram has for some time been used to promote the concept about diminishing fraction of free CO₂ in separate phase, which is considered the most risky part, and thereby increasing safety over time.

The exact amount of CO₂ residing in the different categories of storage mechanisms obviously must be site-specific. The quantification of this over long time spans heavily depends on the ability to simulate the different processes and their interaction for the specific site. The simultaneous simulation of all the processes in question is a demanding task, and has only been carried out for very few storage sites. For the purpose of generating a site specific plot, the published data from a study of a generic case (Zhang et al. 2009) are used in order to illustrate the principles behind the generation of the trapping-mechanism diagram (Frykman et al. 2010).

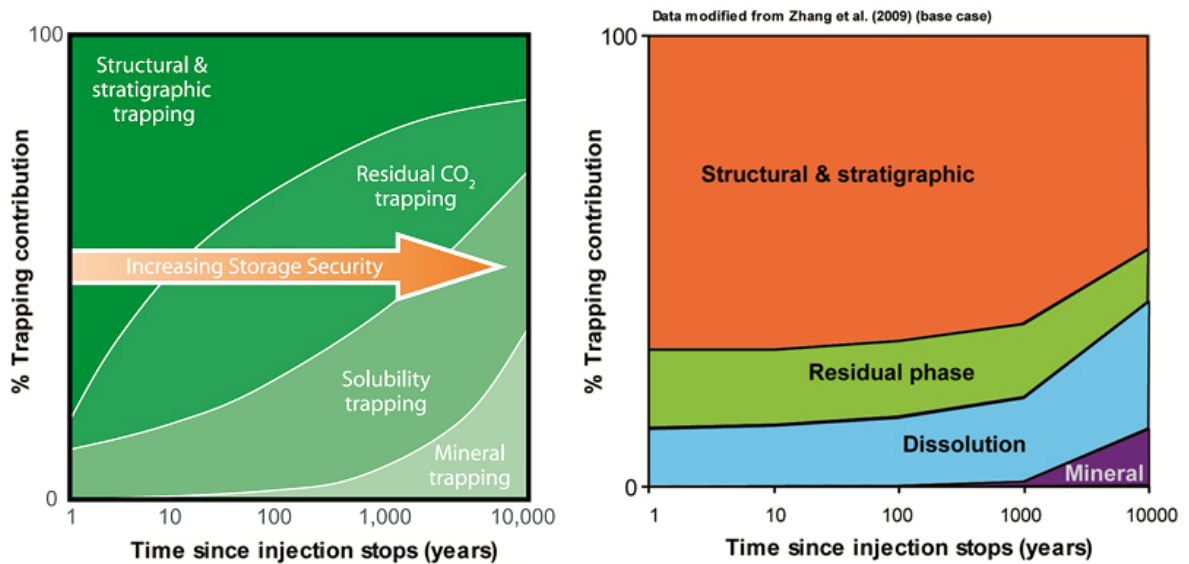


Figure 14: Left) Diagram showing the concept of increasing amount of immobile CO₂, and thereby increased security of the storage facility. The mechanisms responsible for the immobilisation of CO₂ are shown. From IPCC 2005. Right) Trapping-mechanism/time diagram based on data from simulations of the processes of mineral reaction and dissolution. Produced from data given for a base-case study (Zhang et al. 2009). (Figure from Frykman et al. 2010).

The background data for the site specific analysis are derived from the plot of output from using TOUGHREACT to simulate dissolution and mineral trapping contributions (Fig. 13) (Zhang et al. 2009). These data are then re-plotted on the logarithmic time-scale for the safety-time plot. The component of the residual trapped is not simulated explicitly but has to be derived indirectly. Also, the dynamic simulation would not produce the number we are interested in, even if hysteresis were included in the TOUGHREACT simulation. In the context of safety and immobilisation of CO₂, the residual CO₂ is comparable to the concept of residual oil for a produced oil reservoir. The question to answer is how much CO₂ could possibly not escape if we at some time step choose to create maximum leaking conditions for the storage site. For a crude evaluation of this we can then apply the standard hysteresis calculation given that we know the imbibition endpoint for residual CO₂. While this effect is considered formation-specific, it has been demonstrated that residual CO₂ saturations may be as high as 15–25% for many typical storage formations. For the analysed case from (Zhang et al. 2009), the amount of residual CO₂ is not stated and therefore has been deduced using a simple assumption of residual CO₂ saturation of 0.20 as an average for the formation. The assumed 0.20 residual could include two components; the microscopic scale resulting from the pore network properties, and a macroscopic component arising due to heterogenities at larger scale. This results in an estimate of the residual CO₂ at each timestep analysed and corresponds to the capillary trapped non-produceable CO₂ if we were to pressure deplete the storage site.

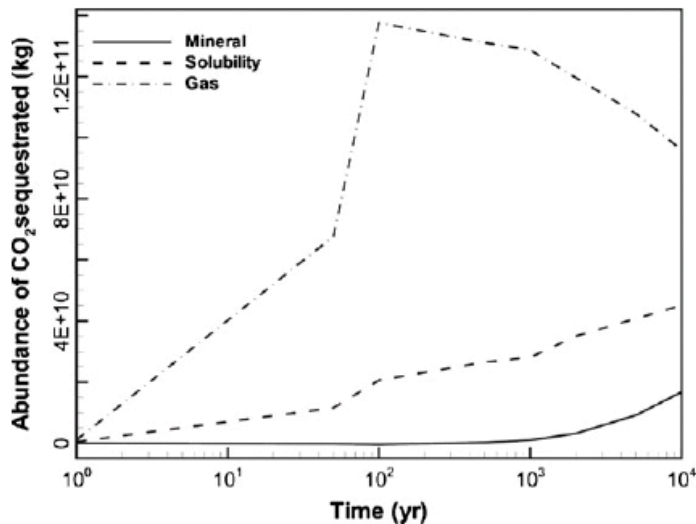


Figure 15: Output diagram from the TOUGHREACT simulation of the base-case by Zhang et al. 2009, forming the basis for the re-calculated proportions.

The simulation of the dissolution process is significantly influenced by the gridding scheme, numerical dispersion and the simulator description of the process. The large amount of dissolved CO₂ reflected in the TOUGHREACT simulation could be caused by these effects as it is usual to operate with instantaneous equilibration for downstream schemes. With large grid cells this implementation cause substantial numerical dispersion and over-estimation of the dissolved part. An evaluation of the estimation of dissolution could incorporate grid convergence testing and an additional assessment of the potential dissolution enhancement due to convective mixing.

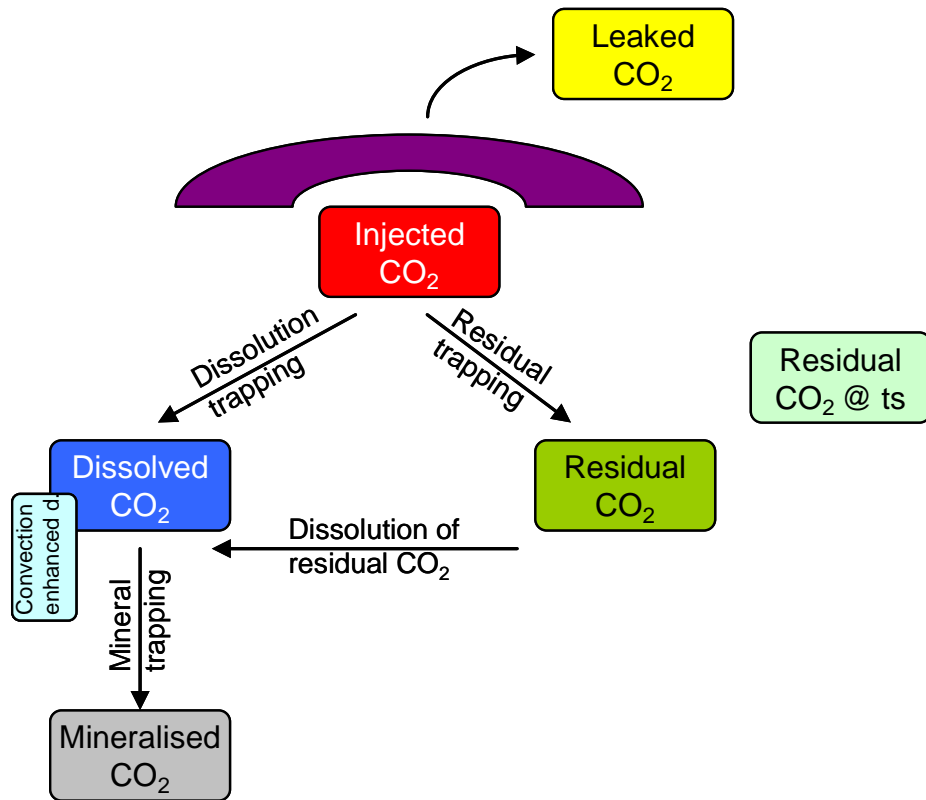


Figure 16: Illustration of the different elements in the trapping of CO₂. All elements except one are formed by the dynamic development of the natural storage site, and the only part we calculate outside the natural processes is the “Residual CO₂ @ts” which is calculated as the residual at a given time-step resulting from optimal production of maximum amount of CO₂ from the storage site. The exact amount can be calculated from a reservoir model by the Land’s equation depending on the maximum saturation reached. Diagram inspired from Tchelepi 2009.



5 Case studies

The following chapter includes summaries and studies of examples from the site portfolio, and describes aspects of the modelling for these specific case studies.

5.1 Reactive transport modelling of CO₂ injection at Sleipner site, North Sea

The Sleipner project is the first commercial scale CO₂ injection project. It was launched in 1996 in a Norwegian offshore saline aquifer located at approximately 1000 m below the seabed and presenting a salinity of 28 g/L. The CO₂ is injected in above the critical point as dense phase in a 200–300 m thick sandstone saline aquifer of the Utsira formation with thinner intermediate horizontal mudstone layers in the reservoir body.

Different models coupling gas and brine flow and chemical interactions were proposed for the simulation of CO₂ injection in Utsira formation. A detailed presentation is only proposed for the last model (Audigane et al., 2007), which considers long-term CO₂ behaviour in a 2D two phase flow reservoir model and complete host-rock (sand and aquifer clay layers). Further models only considered short-term simulations (Johnson et al., 2001; 2004); or were only devoted to the cap rock (Gauss et al., 2005); or considered on limited mineralogy (Frangeul et al., 2004). In the long-term geological storage of carbon dioxide reactive transport model by Audigane et al. (2007), the formation geometry is approximated as a 2D vertical mesh with a cylindrical geometrical configuration centred around an injection point. Five sand layers separated by shale layers were considered

These calculations were carried out using TOUGHREACT code (Xu et al., 2006), which allows the consideration of both reactive geochemical transport and multi-phase fluid flow under non-isothermal conditions. A specific Equation Of State (EOS) fluid property module has been developed for multiphase flow dynamics for CO₂ disposal into saline aquifers (Pruess and Garcia, 2002) and was used by Audigane et al. (2007) for simulating CO₂ injection at Sleipner.

In the few years after starting the CO₂ injection, the dense phase plume, which represents the CO₂, is calculated to extend laterally about 300 m away from the injection point (Figure 17). This extension of the dense phase plume is consistent with the seismic observations. Note that the seismic observations are the most used monitoring methods available at Sleipner injection site (Michael et al., 2010), although injection mass flow data, gravimetric time-lapse surveys and seafloor mapping data are available for Sleipner as well.. In the short term simulations, the presence of the four intra-shale aquitards gives rise to CO₂ accumulations at four different depths and slows the CO₂ upward migration which tends to accumulate at the top of the Utsira formation. After 25 years, the dissolution of dense phase CO₂ in the brine is calculated to produce a maximum dissolved CO₂ mass fraction of 0.052 (Figure 17).

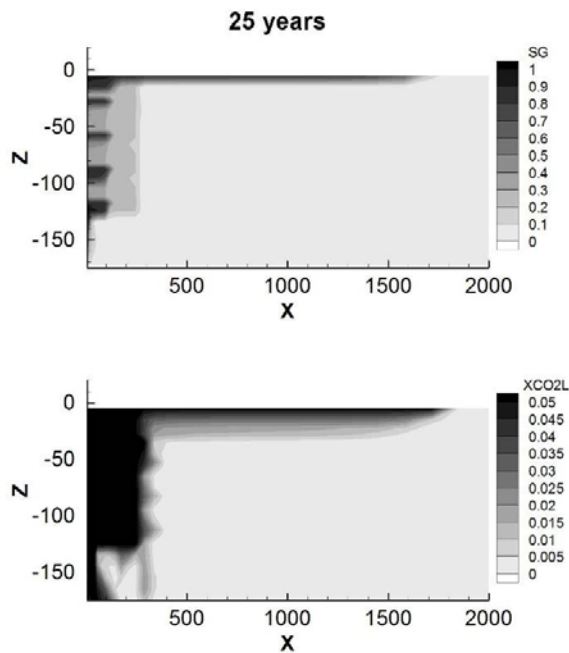


Figure 17: CO₂ dense phase saturation SG (top) and mass fraction of dissolved CO₂ in the porewater XCO2L (bottom), after 25 years of injection (Audigane et al., 2007).

The long term simulation results (Audigane et al., 2007) indicate that the upward migration of the supercritical CO₂ occurs quickly after the end of the injection and most of the CO₂ accumulates at the top of the reservoir formation, just below the cap rock (Figure 18). Some CO₂ is also observed to be residually trapped in the reservoir. In these long term simulations, the CO₂ plume is calculated to extend to a maximum radius of 2000 m from the injection well. CO₂ starts to dissolve in the brine, and the dense phase plume is completely dissolved after 6000 years. The brine with dissolved CO₂ tends to migrate downward as it is approximately 10 kg/m³ denser than brine without CO₂. A convective cell driven by density is calculated to develop, and the brine containing dissolved CO₂ is carried downward and is replaced by brine with lower content in CO₂. After 10000 years, a large volume of brine containing dissolved CO₂ (with a maximum dissolved CO₂ mass fraction of 0.035) is calculated to accumulate at the bottom of the Utsira formation out to a radius of 4000 m (Figure 18). Solubility trapping is predicted to be the main CO₂ trapping mechanism at the Sleipner site over long time scales.

Mineral trapping of CO₂ is calculated to be relatively limited, with only 5% of the injected trapped as a solid phase 10000 years after the injection (Audigane et al., 2007). The CO₂ mineral sinks identified during these calculations are the precipitation of calcite in the shale layers (Figure 19); the alteration of albite, mainly in the shale layers, leading to the formation of dawsonite and chalcedony in the sandstone layers; the precipitation of siderite and dolomite as a result of chlorite and calcite dissolution in the sandstone. Muscovite dissolution is also predicted, enhancing albite and chlorite dissolution.

The main uncertainties of this long-term reactive transport model concern the behaviour of the dense phase CO₂ which is predicted to completely dissolve after 6000 years. Such a complete dissolution is not predicted in other CO₂ injection sites for which long-term reactive transport models have been proposed to study the geochemical trapping of CO₂, like the Gulf Coast sediments, US, (Xu et al., 2003) and the Songlia sandstones, China

(Zhang et al., 2009). This difference in CO₂ behaviour can be explained by the injected amounts of CO₂ in both cases which is 13.2 times higher in the case of the Gulf Coast sediments and 6.6 times higher for the Songlia sandstones case, compared with the Sleipner site case. More confident predictions for the Sleipner site can be obtained considering a more realistic hydrodynamic scenario. Indeed, the development of convective cells in the Utsira formation because of the differences in brine density related to the content in dissolved CO₂ has been pointed out as an important mechanism for brine-rock interactions. However, no regional flow was considered in these calculations and its consideration can modify the geochemical interactions at Sleipner. Other improvements concerns the consideration of Pitzer formalism in the geochemical calculations, more adapted for brines. Performing a sensitivity analysis on the minerals considered in the calculations can also lead to more confident predictions.

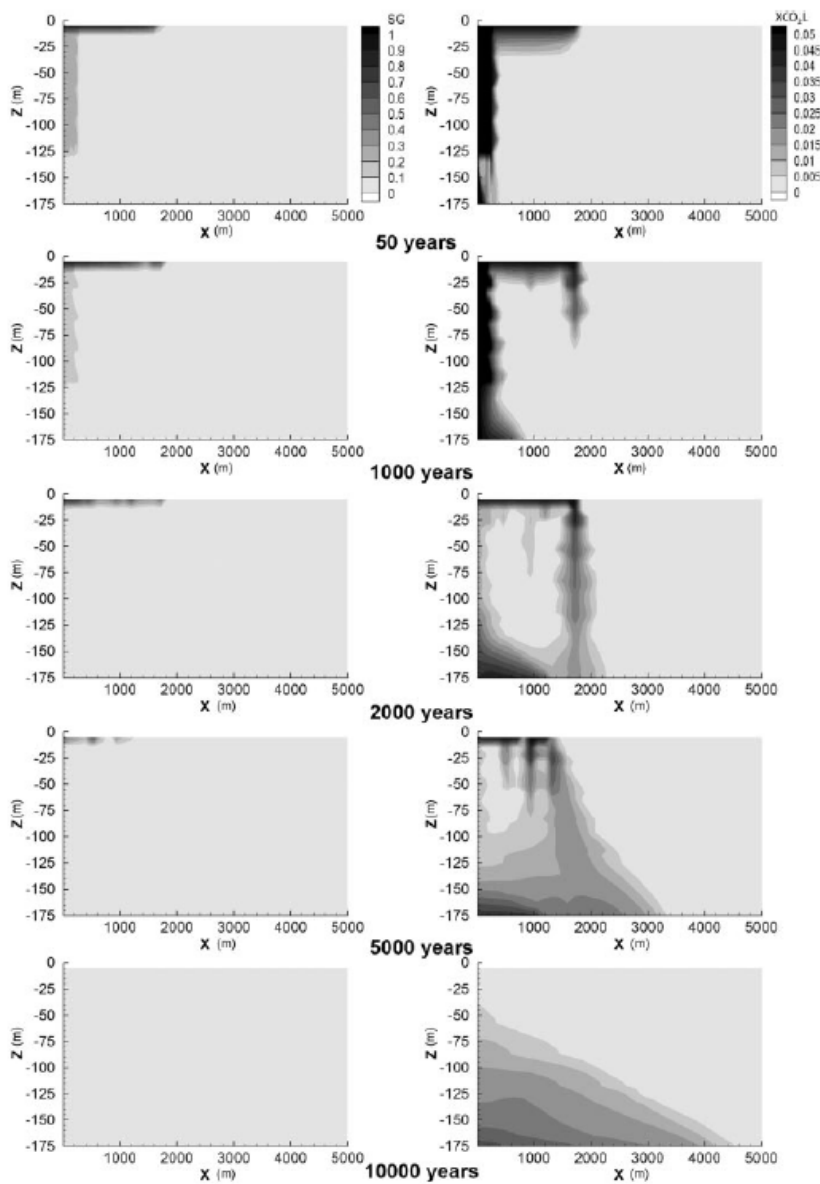


Figure 18: Dense phase CO₂ saturation (SG) and mass fraction of dissolved CO₂ in the porewater (XCO₂L) simulated 50, 1000, 2000, 5000 and 10000 years after injection (Audigane et al., 2007).

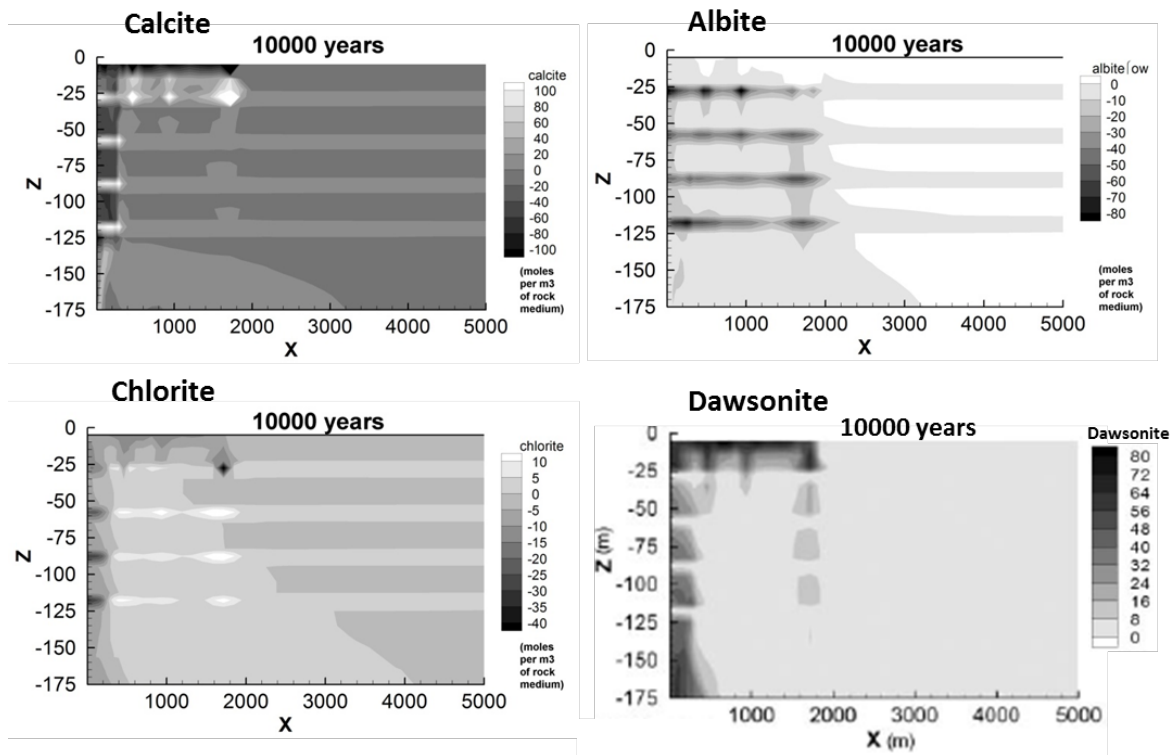


Figure 19: Evolution of calcite, albite, chlorite and dawsonite mineral contents in the Utsira formation, 10000 years after CO₂ injection.

5.2 Reactive transport modelling of CO₂ injection into a methane gas depleted reservoir at the K12-B Field, North Sea

The K12-B field is located in the Dutch sector of the North Sea (150 km away from Amsterdam). It is an offshore methane gas reservoir, exploited by Gaz de France Production Netherland B.V. since 1985. Initially, the gas phase in the reservoir was composed of 13 % of CO₂ and 87 % of CH₄. At present day, K12-B field is almost depleted and is considered for CO₂ storage in the subsurface. The K12-B field is located at a depth of about 3800 m and consists of several tilted fault blocks with little to no fluid flow and pressure communication. It results in a compartmentalization of the individual fault blocks (Van der Meer et al., 2004). At K12-B field, the reservoir is composed by sandstones and claystones units from the early Permian presenting a thickness of about 250 m. Top and side cap-rock consists in shale, carbonate and salt units from the late Permian.

A reactive transport model for compartment 3 of K12-B Field was proposed by Audigane et al. (2009) to simulate the reinjection of CO₂ in the depleted reservoir. The aim of this study was to provide estimates of the amount of the CO₂ remaining as a dense phase CO₂ plume (structural trapping), dissolved into the liquid phase (solubility trapping) and transformed into solid phase (mineral trapping) because of mineral precipitation, during the injection. To overcome computation time limitations, the simulation of CO₂ injection was carried out in two steps: one to simulate the geochemical fluid-rock interaction to assess mineral trapping as well as the cap-rock and sealing integrity of the site; and the second one to estimate structural and solubility trapping of CO₂, without considering geochemical

reactivity. These two separate simulations have been performed using two modules of the heat and fluid flow simulator TOUGH2 (Pruess, 1991). Both simulations carried out by Audigane et al. (2009) have been conducted for a period of 10 yr at an injection rate of 10 kg CO₂/s. It corresponds to the full-scale injection project conditions which consider the injection of about 310,000 to 475,000 tons of CO₂ per year during 10 years. The case considering geochemical fluid-rock interactions highlights the low level of fluid-rock geochemical interactions at the K12-B field. This is explained by the fact that the water formation has already been equilibrated with rock minerals and a large amount of CO₂, since the initial gas phase contained 13% of CO₂. The original geochemical system is acid, and the injection of CO₂ will hardly affect the initial equilibrated chemistry. Minor acidity modifications related to gas saturation modifications are calculated. Four zones are distinguished in the reservoir (Figure 20): (1) the liquid phase saturated part (below the gas-water contact); (2) the gaseous part of the field; (3) the cap-rock; and (4) a region corresponding to a mixing zone located at the gas-water contact area but only within the cap-rock formation. Little mineralogical changes are simulated and are mainly located at the water-gas contact where fluctuations occur because of the pressurization of the reservoir. These mineralogical changes mainly consist in dissolution of muscovite, dolomite and siderite. Near the injection well, small amounts of anhydrite and carbonates are predicted to precipitate, caused by the drying out of the reservoir rock around the injector well. The simulations performed to estimate structural and dissolution trapping indicate an increase of reservoir pressure with CO₂ injection in the depleted reservoir. After 10 years of injection, CO₂ remains at 96 % dense phase, indicating structural trapping is the main process for CO₂ sequestration at the K12-B field at short-term.

Geochemical and 2-phase fluid flow simulations of CO₂ injection in K12-B field suggest this depleted gas reservoir is an excellent candidate for CO₂ geological storage in terms of cap-rock and reservoir integrity (Audigane et al., 2009). The global geochemical reactivity of the system seems to be equilibrated because of the initial presence of CO₂ in the reservoir. At the end of the field-scale CO₂ injection experiment, it will be possible to validate these simulations based on the monitoring of pressure and chemistry evolutions in producer wells.

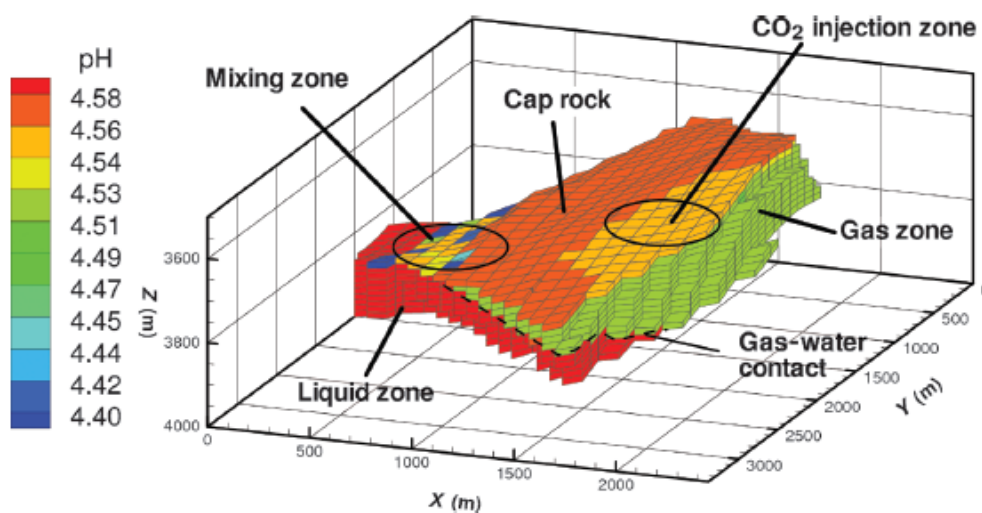


Figure 20: Distribution of the pH values in the reservoir and the first cap-rock after 10 years of CO₂ injection, allowing the distinction of four different zones.

5.3 A preliminary assessment of the contribution of CO₂ trapping mechanisms at the Ketzin pilot site

The contribution of the four CO₂ trapping mechanisms was estimated for the Ketzin pilot site by numerical modelling in two separate steps. In the first step, reservoir modelling was undertaken using the Schlumberger ECLIPSE 100 reservoir simulator (Schlumberger, 2009) based on the latest version of the history matched static geological model of the Stuttgart Formation as implemented in the CO₂MAN project funded by the German Ministry of Education and Research (BMBF) and industry funding. The second step of the present approach comprises geochemical batch simulations using the PHREEQC simulator (Parkhurst and Appelo, 1999) taking into account the fluid and mineral composition as determined by well sampling at the Ketzin pilot site as well as data on the dissolved CO₂ mass and water saturation from the reservoir simulations undertaken in the first step. The procedure used in this study is reasonable, since relevant mineral alteration takes place several hundred years after the hydraulic equilibrium with regard to CO₂ migration.

5.3.1 Assessment of CO₂ dissolution by reservoir simulations

Reservoir simulations parameterized as discussed by Kempka et al. (2010) were performed up to the year 2300 on a revised model of the Stuttgart formation and allowed us for an estimation of the time-dependent development of CO₂ dissolution, whereas the gas phase is assumed to be structurally trapped. The residual gas saturation of 0.05 was considered for the estimation of the contribution of residual trapping at elements where gaseous CO₂ is present at for all timesteps, since hysteresis effects were not taken into account in the present simulation runs. Figure 21 shows the CO₂ saturation at the Ketzin pilot site after an injection of about 70,000 t of CO₂ up to April 2013 at the end of the year 2300. The CO₂ plume migrated dip-upward to the top of the anticline and is being structurally trapped due to a present fault offset and the initial assumption that the caprock is impermeable and the fault is not permeable in vertical direction.

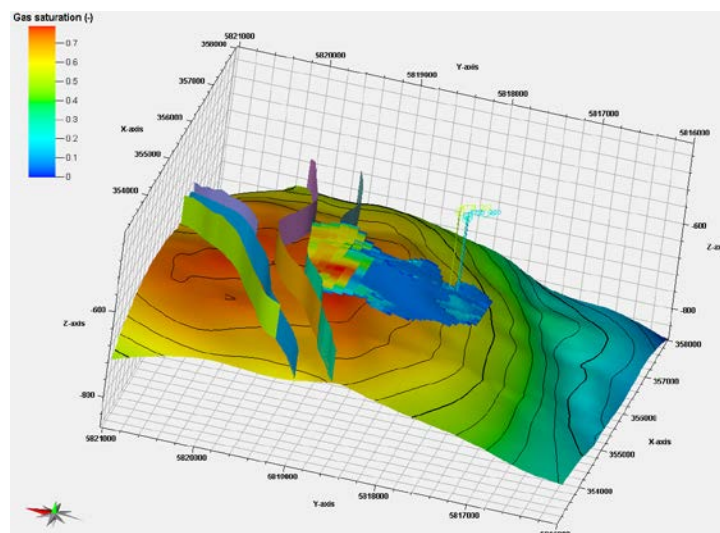


Figure 21: Spatial distribution of the CO₂ plume at the Ketzin site in 2300 under the assumption of 70,000 t CO₂ being injected until the end of April 2013.

Figure 22 a) and b) show the spatial distribution and saturation of the gaseous and dissolved CO₂ plume at the Ketzin pilot site in 2300. The reservoir simulation results were compiled and analysed for the implementation into the geochemical batch simulations.

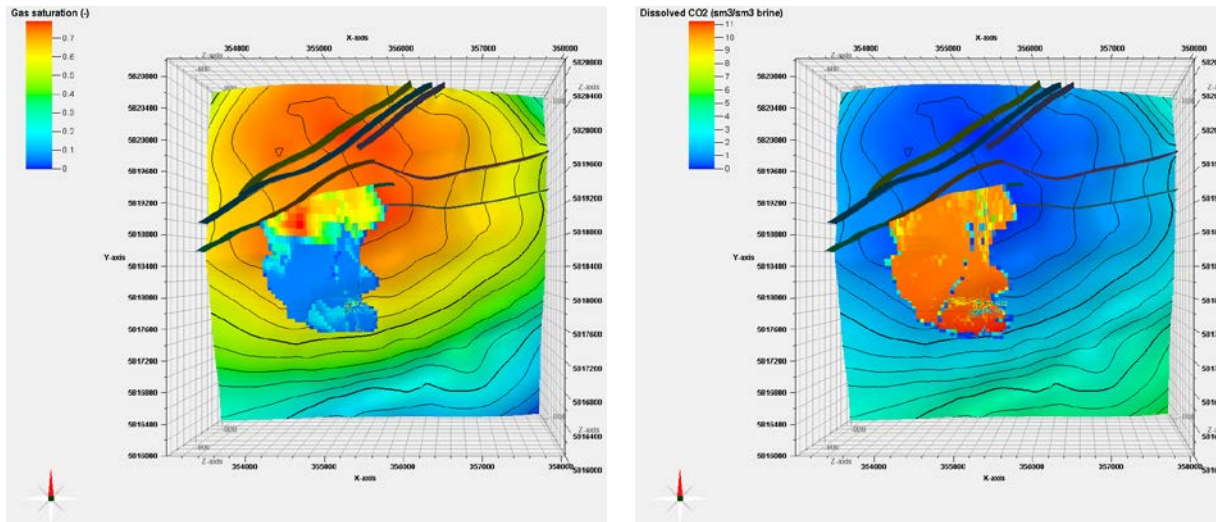


Figure 22: Spatial distribution of dense phase (left) and dissolved CO₂ (right) at the Ketzin pilot site in 2300.

5.3.2 Geochemical model parametrisation

Initial mineralogy is based on modal mineralogy estimated from point-count analysis (Förster et al. 2010; Norden et al. 2010). Since the measured composition cannot be introduced as such in a geochemical model, some minerals were excluded, others included as a proxy or secondary mineral. For the selection, reactivity, abundance and availability of data of each mineral were taken into account. Table 2 shows the minerals considered in the model; the rest - mainly quartz – is therefore considered inert.

Table 2: Primary minerals introduced into the model based on Förster et al. (2010) and Norden et al. (2010).

Primary Minerals	wt.%
K-feldspar	9.32
Albite	26.55
Illite	6.79
Chlorite	5.24
Anhydrite	4.21
Hematite	1.00

Initial brine composition (Table 3) is calculated based on chemical analysis of reservoir fluid samples (Förster et al., 2006; Würdemann et al., 2010; unpublished data), while equilibrium with primary minerals (albite, illite, chlorite, hematite) was assumed. Secondary minerals which are allowed to precipitate are calcite, dolomite, kaolinite, magnesite, pyrite and siderite.

Table 3: Initial brine composition introduced into the model based on reservoir fluid sample analysis (Förster et al., 2006; Würdemann et al., 2010 and unpublished data).

Fluid Modell [mol/kgw]	
Temperature [°C]	35
pH	6.6
pe	-2.15
Error [%] in electrical balance	-0.5
Al	1.28E-08
C (4)	9.65E-04
Ca	5.67E-02
Cl	4.34E+00
Fe	1.05E-04
K	1.03E-02
Mg	4.06E-02
Na	4.188
S (6)	4.45E-02
Si	1.43E-04

Apart from calcite, which is always considered at equilibrium with the brine, dissolution and precipitation of all minerals proceed under kinetic conditions. The rate equation from Lasaga et al. (1994) considering multiple mechanisms (neutral, acid and base) is used, desuming rate law parameters from Palandri & Kharaka (2004) (Table 4). Illite and chlorite kinetic data are set to those of muscovite and clinocllore in each case. Pyrite kinetic data are taken from Xu et al. (2010). Reactive surface areas for dissolution are calculated from the geometric surface area assuming spherical mineral grains.

Table 4: Kinetic rate parameters taken from Palandri and Kharaka (2004), in case of Pyrite from Xu et al. (2010).

	Neutral mechanism		Acid mechanism			Base mechanism		
	logk25	Ea	logk25	Ea	n(H+)	logk25	Ea	n(H+)
Primary minerals								
K-feldspar	-12.41	38	-10.06	51.7	0.5	-21.2	94.1	-0.823
Albite	-12.56	69.8	-10.16	65	0.457	-15.6	71	-0.572
Illite	-13.55	22	-11.85	22	0.37	-14.55	22	-0.22
Chlorite	-12.52	88	-11.11	88	0.5			
Anhydrite	-3.19	14.3						
Hematite	-14.6	66.2	-9.39	66.2	1			
Secondary minerals								
Calcite	Equilibrium							
Dolomite (dis.)	-7.53	52.2	-3.19	36.1	0.5	-5.11	34.8	0.5
Kaolinite	-13.18	22.2	-11.81	65.9	0.777	-17.05	17.9	-0.472
Magnesite	-9.34	23.5	-6.38	14.4	1	-5.22	62.8	1
Pyrite	-4.55	56.9	-7.52	56.9	-0.5			
Siderite	-8.9	62.76	-3.747	48	0.75			

5.3.3 Geochemical modelling results

Geochemical batch simulations were run using the code PHREEQC (Parkhurst and Appelo, 1999) and the LLNL thermodynamic database, under the assumption that the amount of dissolved CO₂ corresponds to equilibrium with a constant pressure of the CO₂ gas phase in contact with the solution. The pressure itself was found to have a negligible impact on mineral alterations, at least in the considered range of 55 bar to 76 bar as expected for the Ketzin pilot site, and thus is only of relevance in the calculation of the amount of dissolved CO₂. Figure 23 shows the result of an exemplary simulation scaled to 1 m³ of rock with a porosity of 18 % and water saturation of 99 %, corresponding to the presence of a very small amount of gaseous CO₂ present in the pore volume. Decreasing the water saturation in a reference volume lets a smaller amount of solution “see” the same mineral reactive surfaces, so that reactions are faster but also quantitatively smaller. Simulation results indicate the precipitation of Kaolinite and K-feldspar, compensated by the dissolution of illite, chlorite, anhydrite and, initially, albite. Subsequently, albite reverts its saturation state and starts precipitating again after about 100 years. By the end of the simulations, the total amount of albite in the rock has increased. The pH of the solution initially decreases to around 3 to steadily increase afterwards until it reaches about 4.5. At that point – after about 1,000 years in the simulation illustrated in Figure 23 – siderite starts to precipitate.

Of all carbonate minerals included in the model (siderite, calcite, magnesite and dolomite), siderite is the only which precipitates, and thus mainly contributes to mineral trapping. For comparison, water saturation of 50% leads siderite precipitating to start after 600 years.

The total change in the mineral volume after 3.000 years which amounts to about -150 cm³/m³, can be considered insignificant in terms of porosity changes and thus with regard to hydraulic flow processes in the reservoir.

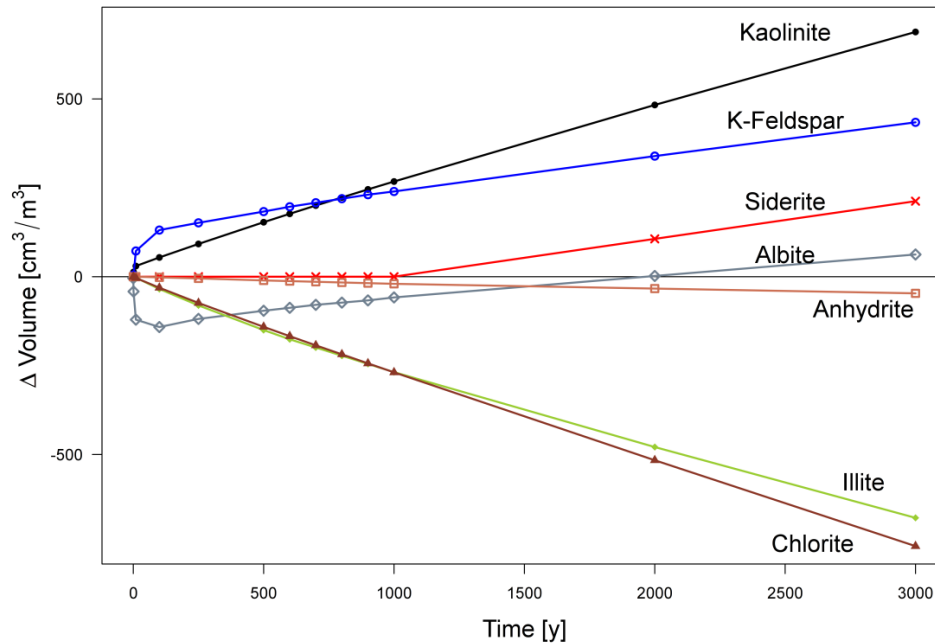


Figure 23: Changes in mineral volumes resulting from geochemical simulations, in cm³/m³ of rock.

5.3.4 Contribution of trapping mechanisms

The contribution of structural, residual and dissolution trapping were determined by reservoir simulations up to the year 2300. Data for structural and dissolution trapping was estimated by fitting based on the simulated data for years 2200 to 2300 and predicting the future behavior up to the year 5000. Geochemical batch simulations were performed for the entire investigated time span of 3000 years.

Figure 24 shows the total contribution of the four CO₂ trapping mechanisms calculated for the Ketzin pilot site. In 2420 about 50 % of CO₂ is dissolved in the Stuttgart formation, while the dissolution ratio increases to about 54.3 % in 5000. Residual trapped CO₂ was assumed to be present in elements determined by the presence of a free gas phase, whereas the residual gas saturation of $S_{gr} = 0.05$ measured for the average lithofacies in the Stuttgart formation was applied to calculate the cumulative related residual trapping for elements with a free gas phase present. Residual trapping decreases after CO₂ has migrated dip-upwards due to CO₂ dissolution, and then slightly increases with the presence of a free gas phase at the top of the anticline.

Assuming the pore volume to be almost fully saturated with the formation fluid, first mineralization processes in form of siderite precipitation start in 3000 and linearly increase to a mineralized amount of 9.4 % of the injected CO₂ in 5000. Porosity changes relevant for dynamic reservoir behavior are not to be expected in the Stuttgart formation according to the geochemical simulation results.

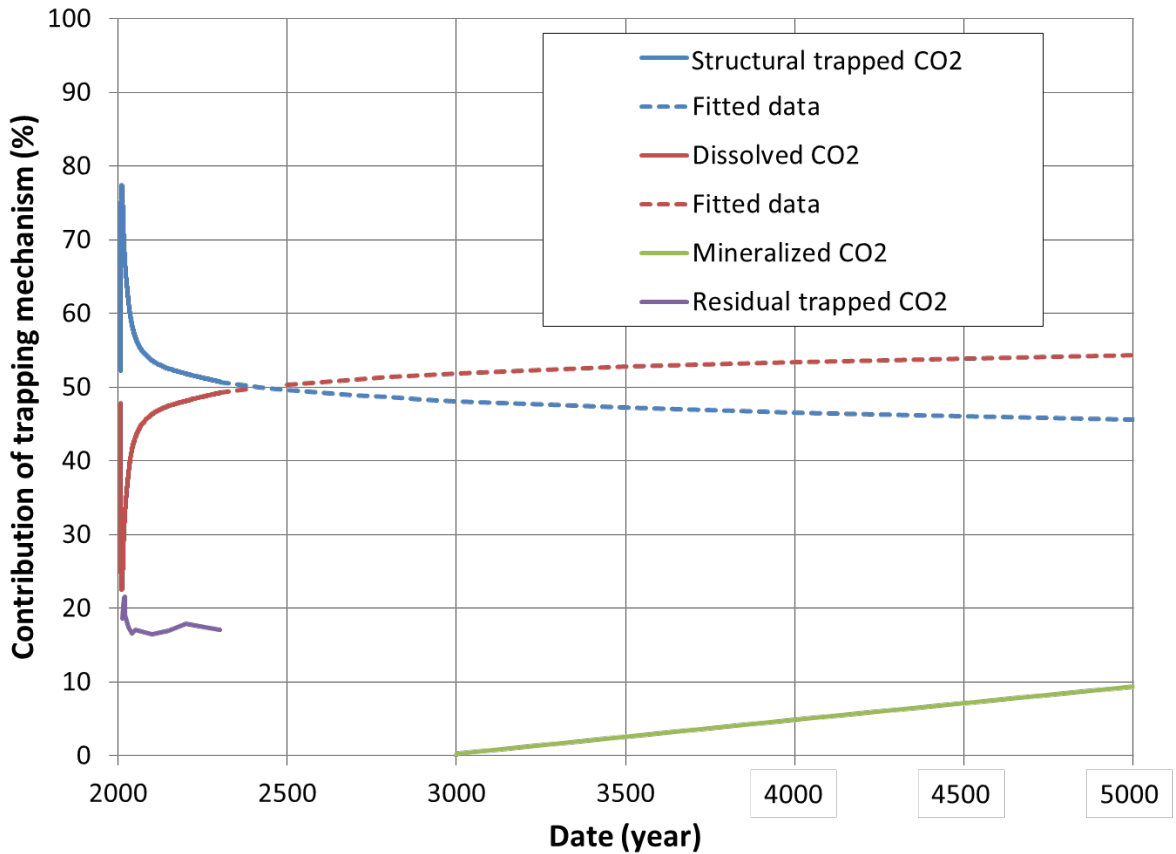


Figure 24: Contribution of the four CO₂ trapping mechanisms, whereas the residual trapped CO₂ ratio is included in the gas phase (structural trapped CO₂) and the mineralized CO₂ ratio in the dissolved CO₂ (structural trapped and dissolved CO₂ sum up to 100%).

Reservoir simulations addressing times beyond 2300 were not undertaken due to limited computational resources. However, these simulations are in preparation to improve the knowledge on the dissolution and residual trapping ratio development at the Ketzin pilot site. Including hysteresis effects into the reservoir simulations is scheduled as soon as laboratory measurements on cores from the Ketzin pilot site reveal reliable results, since estimation of residual trapping is currently considered very conservative, since it does not take into account snap-off effects as a result of the dip-upward migration and related imbibition. In addition, geochemical simulations suffered from convergence problems beyond the year 5000. For that purpose, we intend to revise our selection of secondary minerals and reduce their amount in order to overcome convergence problems and allow for long-term simulations up to 10,000 years.

6 References

- Al-Futaisi, A., and T. W. Patzek (2003), Impact of wettability on two-phase flow characteristics of sedimentary rock: A quasi-static description, *Water Resour. Res.*, 39(2), 1042, doi:10.1029/2002WR001366.
- Audigane, P., J. Lions, I. Gaus, C. Robelin, P. Durst, B. Van der Meer, K. Geel, C. M. Oldenburg, and T. Xu (2009), Geochemical modeling of CO₂ injection into a methane gas reservoir at the K12-B Field, North Sea, in *Carbon dioxide sequestration in geological media - State of the science*, edited by M. Grobe, J. C. Pashin and R. L. Dodge, pp. 499-519.
- Audigane, P., Gaus, I., Czernichowsky-Lauriol, I., Pruess, K., Xu, T. Two-dimensional reactive transport modeling of CO₂ injection in a saline aquifer at the Sleipner site, 2007. North Sea, *American Journal of Science*, 2007, Vol. 307, pp. 974 – 1008.
- Bachu, S., Bonijoly, D., Bradshaw, J., Burruss, R., Holloway, S., Christensen, N.P. & Mathiassen, O.M. 2007. CO₂ storage capacity estimation: Methodology and gaps *International Journal of Greenhouse Gas Control*, 2007, Vol. 1(4), pp. 430 – 443.
- Cantucci, B., Montegrossi, G., Vaselli, O., Tassi, F., Quattrocchi, F. & Perkins, E.H. 2009. Geochemical modeling of CO₂ storage in deep reservoirs: The Weyburn Project (Canada) case study *Chemical Geology*, 2009, Vol. 265(1-2), pp. 181 – 197.
- Bachu, S. & Bennion, B. 2007 Effects of in-situ conditions on relative permeability characteristics of CO₂ –brine systems *Environmental Geology*, Volume 54, Issue 8, pp.1707-1722. doi 10.1007/s00254-007-0946-9.
- Bachu S., Bonijoly D., Bradshaw J., Burruss R., Holloway S., Christensen N.P., Mathiassen O.M. (2007) CO₂ storage capacity estimation: Methodology and gaps, *Int. J. Greenhouse Gas Control* 1, pp. 430-443.
- Bachu, S., Adams, J.J.. 2003. Sequestration of CO₂ in geological media in response to climate change: capacity of deep saline aquifers to sequester CO₂ in solution. *Energy Conversion and Management* 44 (2003) pp. 3151–3175.
- Benson, S.M., Cook, P.J., 2005. Underground geological storage of carbon dioxide. In: Metz, B., et al. (Eds.), *Intergovernmental Panel on Climate Change Special Report on Carbon Dioxide Capture and Storage*. Cambridge University Press, pp. 195–276 (Chapter 5).
- Bergmo, P. Grimstad, A., Lindeberg, E., Riis, F., Johansen, W.T.. 2009. Exploring geological storage sites for CO₂ from Norwegian gas power plants: Utsira South. *Energy Procedia* 1, pp. 2953-2959.
- Chadwick A., Arts R., Bernstone C., May F., Thibeau S., Zweigel P. (eds) (2008) *Best practice for the storage of CO₂ in saline aquifers, Observations and guidelines from the SACS and CO2STORE projects*, Keyworth, Nottingham, BGS Occasional Publication No. 14.



- CO2CRC, 2008. Storage Capacity Estimation, Site Selection and Characterisation for CO₂ Storage Projects. Cooperative Research Centre for Greenhouse Gas Technologies, Canberra. CO2CRC Report No. RPT08-1001. 52pp. Edited by: J. G. Kaldi¹ and C. M. Gibson-Poole, CO2CRC.
- Ennis-King J., Paterson L. (2003) Role of convective mixing in the long-term storage of carbon dioxide in deep saline formations, SPE paper 84344 presented at SPE ATCE, Denver, Colorado, USA, 5-8 October, 2003.
- Ennis-King, J., Paterson, L. 2003a. Rate of dissolution due to convective mixing in the underground storage of carbon dioxide. In: Gale, J., Kaya, Y. (eds.) Greenhouse Gas Control Technologies, vol. 1, pp. 507–510, Elsevier, Amsterdam (2003a).
- Ennis-King, J., Paterson, L. 2003b. Role of convective mixing in the long-term storage of carbon dioxide in deep saline formations. Paper SPE-84344 presented at Society of Petroleum Engineers Annual Fall Technical Conference and Exhibition, Denver, CO, October.
- Ennis-King, J., Preston, I., Paterson, L. 2005. Onset of convection in anisotropic porous media subject to a rapid change in boundary conditions. *Phys. Fluids* 17, 084107 (2005). doi:10.1063/1.2033911.
- Frangeul et al., 2004 J. Frangeul, L. Nghiem, C. Emmanuel and S. Thibeau, Sleipner/Utsira CO₂ geological storage: full field flow and geochemical coupling to assess the long term fate of the CO₂ Proceedings AAPG Annual Conference, Paper AAPG 86278 Dallas, TX, 18–21 April (2004).
- Frykman, P., Nielsen, C.M., Dalhoff, F., Sørensen, A.T., Klinkby, L. and Nielsen, L.H.: 2010. Geological modelling for site evaluation at the Vedsted structure, NW Denmark. GHGT-10, Proceedings of the 10th International Conference on Greenhouse Gas Control Technologies.
- Förster, A., Norden, B., Zinck-Jorgensen, K., Frykman, P., Kulenkampff, J., Spangenberg, E., Erzinger, J., Zimmer, M., Kopp, J., Borm, G., Juhlin, C., Cosma, C.-G., Hurter, S., 2006. Baseline characterization of the CO₂SINK geological storage site at Ketzin, Germany, *Environmental Geosciences* 13, pp. 145-161.
- Förster, A., Schöner, R., Förster, H.-J., Norden, B., Blaschke, A.-W., Luckert, J., Beutler, G., Gaupp, R., Rhede, D., 2010. Reservoir characterization of a CO₂ storage aquifer: The Upper Triassic Stuttgart Formation in the Northeast German Basin. *Marine and Petroleum Geology* 27, pp. 2156-2172.
- Garcia, J. 2001. Density of Aqueous Solutions of CO₂. Lawrence Berkeley National Laboratory Report LBNL- 49023, Berkeley, CA (2001).
- Gaus, I. 2010. Role and impact of CO₂ -rock interactions during CO₂ storage in sedimentary rocks *International Journal of Greenhouse Gas Control*, 2010, Vol. 4(1), pp. 73 – 89.

- Gaus, I., Audigane, P., André, L., Lions, J., Jacquemet, N., Durst, P., Czernichowski-Lauriol, I. & Azaroual, M. 2008. Geochemical and solute transport modelling for CO₂ storage, what to expect from it? *International Journal of Greenhouse Gas Control*, 2008, Vol. 2(4), pp. 605 – 625.
- Gaus, I., Azaroual, M. & Czernichowski-Lauriol, I. 2005. Reactive transport modelling of the impact of CO₂ injection on the clayey cap rock at Sleipner (North Sea) *Chemical Geology*, 2005, Vol. 217(3-4), pp. 319 – 337.
- Gaus, I., Guern, C.L., Pearce, J., Pauwels, H., Shepherd, T., Hatzilynnis, G. & Metaxas, A. 2008. Comparison of long-term geochemical interactions at two natural CO₂ - analogues: Montmiral (Southeast Basin, France) and Messokampos (Florina Basin, Greece) case studies. Rubin, E., Keith, D., Gilboy, C., Wilson, M., Morris, T., Gale, J. & Thambimuthu, K. (ed.) *Greenhouse Gas Control Technologies 7 Elsevier Science Ltd*, 2005 (2), pp. 561 – 569.
- Gudogan, O., Mackay, E. & Todd, A. 2011. Comparison of numerical codes for geochemical modelling of CO₂ storage in target sandstone reservoirs *Chemical Engineering Research and Design*, 2011, Vol. 89(9), pp. 1805 – 1816.
- Hellevang, H., Aagaard, P., Oelkers, E.H., Kvamme, B. 2005. Can Dawsonite Permanently trap CO₂? *Environmental Science Technology*, 2005, Vol. 39, pp. 8281– 8287.
- Hesse, M.A., Tchelepi, H.A., Orr, Jr. F.M. 2006. Natural convection during aquifer CO₂ storage. Presented at 8th International Conference on Greenhouse Gas Control Technologies, Trondheim, Norway, June 2006.
- Hesse et al. 2008. Gravity currents with residual trapping. *J. Fluid Mech.* (2008), vol. 611, pp. 35–60.
- Hu, J., Duan, Z., Zhu, C., Chou, I-M. 2007. PVTx properties of the CO₂ –H₂O and CO₂ – H₂O–NaCl systems below 647 K: Assessment of experimental data and thermodynamic models. *Chemical Geology* 238, pp. 249–267.
- IPCC 2005. Special Report on Carbon Dioxide Capture and Storage, Prepared by Working Group III of the Intergovernmental Panel on Climate Change, Cambridge University Press, Cambridge, United Kingdom and New York, NY, USA, 442 pp.
- Ide, S. T., Jessen, K. & Orr, Jr, F. M. 2007. Storage of CO₂ in saline aquifers: effects of gravity, viscous, and capillary forces on amount and timing of trapping. *Intl J. Greenh. Gas Control* 1(4), pp. 481–491.
- Johnson, J.W., J.J. Nitao, C. Steefel and K.G. Knaus, 2001. Reactive transport modelling of geological CO₂ sequestration in saline aquifers; The influence of intra-aquifer shales and the relative effectiveness of structural, solubility, and mineral trapping during prograde and retrograde sequestration First Annual Conference on Carbon Sequestration Washington, 14–17 May (2001).
- Johnson, J.W., Nitao, J.J., Knauss, K.G. 2004. Reactive transport modelling of CO₂ storage in saline aquifers to elucidate fundamental processes, trapping mechanisms

- and sequestration partitioning. Geological Society, London, Special Publications, 2004, Vol. 233, pp. 107–128.
- Juanes, R., Spiteri, E. J., Orr, Jr, F. M. & Blunt, M. J. 2006. Impact of relative permeability hysteresis on geological CO₂ storage. *Water Resour. Res.* 42 (W12418), pp. 1–13.
- Kempka, T., Kühn, M., Class, H., Frykman, P., Kopp, A., Nielsen, C.M., Probst, P., 2010. Modelling of CO₂ arrival time at Ketzin - Part I. *International Journal of Greenhouse Gas Control*, Special Issue Geological CO₂ Storage 4(6):1007-1015
- Kneafsey, T.J. and Pruess, K. 2011. Laboratory Flow Experiments for Visualizing Carbon Dioxide-Induced, Density-Driven Brine Convection, *Transport in Porous Media* 82, pp. 123-139. DOI 10.1007/s11242-009-9482-2.
- Labus, K. & Bujok, P. 2011. CO₂ mineral sequestration mechanisms and capacity of saline aquifers of the Upper Silesian Coal Basin (Central Europe) - Modeling and experimental verification *Energy*, 2011, Vol. 36(8), pp. 4974 – 4982.
- Land, C.S.1968. "Calculation of Imbibition Relative Permeability for Two- and Three-Phase Flow from Rock Properties," *Soc. Pet. Eng. J.*, Vol. 8, No. 2 (June 1968) pp. 149-156.
- Lasaga, A.C., Soler, J.M., Ganor, J., Burch, T.E., Nagy, K.L., 1994. Chemical weathering rate laws and global geochemical cycles. *Geochim. Cosmochim. Acta* 58, pp. 2361-2386
- Lenormand, R., C. Zarcone, and A. Sarr (1983), Mechanisms of the displacement of one fluid by another in a network of capillary ducts, *J. Fluid Mech.*, 135, pp. 123–132.
- Lindeberg, E., Wessel-Berg, D.1997. Vertical convection in an aquifer column under a gas cap of CO₂. *Energy Convers. Manag.* 38 (Suppl), S229–S234.
- Lindeberg, E., Bergmo, P.2003. The long-term fate of CO₂ injected into an aquifer. In: Gale, J., Kaya, Y. (eds.) *Greenhouse Gas Control Technologies*, pp. 489–494. Elsevier Science Ltd, Amsterdam, The Netherlands (2003).
- Liu, N., Liu, L., Qu, X., Yang, H., Wang, L. & Zhao, S. 2011. Genesis of authigenic carbonate minerals in the Upper Cretaceous reservoir, Honggang Anticline, Songliao Basin: A natural analog for mineral trapping of natural CO₂ storage *Sedimentary Geology*, 2011, Vol. 237(3-4), pp. 166 – 178.
- Mansoori, S.A, Iglauer, S., Pentland, B.B. and Blunt, M.J. 2009. Measurements of Non-Wetting Phase Trapping Applied to Carbon Dioxide Storage. *Energy Procedia* 1, pp. 3173-3180.
- Michael, K., M. Arnot, P. Cook, J. Ennis-King, R. Funnell, J. Kaldi, D. Kirste, and L. Paterson (2010), CO₂ storage in saline aquifers I—Current state of scientific knowledge, *Energy Procedia*, 1(1), pp. 3197-3204.
- Mo, S., Zweigel, P., Lindeberg, E. & Akervoll, I. 2005 Effect of geologic parameters on CO₂ storage in deep saline aquifers. In *SPE Eurospec/EAGE Annu. Conf. Madrid, Spain*.

- Nghiem, L., Yang, C., Shrivastava, V., Kohse, B., Hassam, M. and Card, C. 2009. Risk Mitigation Through the Optimization of Residual Gas and Solubility Trapping for CO₂ Storage in Saline Aquifers. *Energy Procedia* 1, pp. 3015-3022.
- Norden, B., Förster, A., Vu-Hoang, D., Marcelis, F., Springer, N., Le Nir, I., 2010. Lithological and petrophysical core-log interpretation in CO₂SINK, the European CO₂ onshore research storage and verification project. *SPE Reservoir Evaluation & Engineering* 13, pp. 179-192.
- Oak, M. J. (1990), Three-phase relative permeability of water-wet Berea, SPE Pap. 20183-MS, Soc. of Pet. Eng., Richardson, Tex, (SPE/DOE 20183).
- Palandri, J., Kharaka, Y.K., 2004. A compilation of rate parameters of water-mineral interaction kinetics for application to geochemical modeling. US Geol. Surv. Open File Report 2004-1068. 64pp.
- Parkhurst, D.L., Appelo, C.A.J., 1999. User's guide to PHREEQC (version 2) - a computer program for speciation, reaction-path, 1D-transport, and inverse geochemical calculations. US Geol. Surv. Water Resour. Inv. Rep. 99-4259, 312 p.
- Pickup, G.E., M. Kiatsakulphan, and J.R. Mills. 2010. Analysis of Grid Resolution for Simulations of CO₂ Storage in Deep Saline Aquifers. 12th European Conference on the Mathematics of Oil Recovery, 2010, Oxford.
- Pruess, K., and J. García (2002), Multiphase flow dynamics during CO₂ disposal into saline aquifers, *Environmental Geology*, 42(2), pp. 282-295.
- Riaz, A., Hesse, M., Tchelepi, H.A., Orr, Jr. F.M. 2006. Onset of convection in a gravitationally unstable diffusive boundary layer in porous media. *J. Fluid Mech.* 548, pp. 87–111 (2006).
- Riazi, M., Sohrabi, M., Bernstone, C., Jamiolahmady, M., Ireland, S., (2011). Visualisation of mechanisms involved in CO₂ injection and storage in hydrocarbon reservoirs and water-bearing aquifers. *Chemical Engineering Research and Design* CHERD-750, Elsevier.
- Sato K., Mito, S., Horie, T., Ohkuma, H., Saito, H., Watanabe, J., Yoshimura, T.. 2011. Monitoring and simulation studies for assessing macro- and meso-scale migration of CO₂ sequestered in an onshore aquifer: Experiences from the Nagaoka pilot site, Japan. *International Journal of Greenhouse Gas Control* 5 (2011) pp. 125–137.
- Schlumberger, 2009. Schlumberger, Eclipse Technical Manual, (2009).
- Soong, Y., Goodman, A.L., McCarthy-Jones, J.R. & Baltrus, J.P. 2004. Experimental and simulation studies on mineral trapping of CO₂ with brine *Energy Conversion and Management*, 2004, Vol. 45(11-12), pp. 1845 – 1859.
- Spiteri, E. J., R. Juanes, M. J. Blunt, and F. M. Orr Jr. (2005), Relative permeability hysteresis: Trapping models and application to geological CO₂ sequestration, in *SPE Annual Technical Conference and Exhibition*, Dallas, TX, (SPE 96448).



- Tchelepi, H. 2009: CO₂ Sequestration in Deep Saline Aquifers: What are the Relevant Length and Time Scales. Energy Resources Engineering, Stanford, SIAM Lecture Series, Stanford.
- Thibeau, S. and Mucha, V. 2011. Have We Overestimated Saline Aquifer CO₂ Storage Capacities? Oil & Gas Science and Technology – Rev. IFP Energies nouvelles, Vol. 66 (2011), No. 1.
- Valvatne, P. H., and M. J. Blunt (2004), Predictive pore-scale modeling of two-phase flow in mixed wet media, Water Resour. Res., 40, W07406, doi:10.1029/2003WR002627.
- Van der Meer, L. G. H., E. Kreft, C. Geel, and J. Hartman, 2004, K12-B test site for CO₂ storage and enhanced gas recovery: 14th Europec Biennial Conference, Madrid, Spain, June 13–16, 2004, Society of Petroleum Engineers Paper No. 94128, 12 p.
- van der Meer L.G., van Wees J.D. (2006) Limitations to storage pressure in finite saline aquifers and the effect of CO₂ solubility on storage pressure, SPE paper 103342, presented at SPE ATCE held, San Antonio, Texas, USA, 24-27 September 2006.
- Weir G.J., White S.P., Kissling W.M.1995. Reservoir storage and containment of greenhouse gases. In: Pruess K. (ed.) Proceedings of the TOUGH Workshop '95, pp. 233–238. Lawrence Berkeley National Laboratory Report LBL-37200, Berkeley, CA (1995).
- Weir, G.J., White, S.P., Kissling, W.M.1996. Reservoir storage and containment of greenhouse gases. Transp. Porous Media 23, pp. 37–60 (1996).
- Worden, R.H. 2006. Dawsonite cement in the Triassic Lam Formation, Shabwa Basin, Yemen: A natural analogue for a potential mineral product of subsurface CO₂ storage for greenhouse gas reduction Marine and Petroleum Geology, 2006, Vol. 23(1), pp. 61 – 7.
- Würdemann, H., Möller, F., Kühn, M., Heidug, W., Christensen, N.-P., Borm, G., Schilling, F.-R., CO2SINK Group, 2010. CO2SINK- From site characterization and risk assessment to monitoring and verification: One year of operational experience with the field laboratory for CO₂ storage at Ketzin, Germany. International Journal of Greenhouse Gas Control 4, pp. 938-951.
- Xu, T., E. Sonnenthal, N. Spycher, and K. Pruess (2006), TOUGHREACT—A simulation program for non-isothermal multiphase reactive geochemical transport in variably saturated geologic media: Applications to geothermal injectivity and CO₂ geological sequestration, Computers & Geosciences, 32(2), pp. 145-165.
- Xu, X., Chen, S., Zhang, D. 2006. Convective stability analysis of the long-term storage of carbon dioxide in deep saline aquifers. Adv. Wat. Resour. 29, pp. 397–407 (2006).
- Xu, T., Apps, J.A. & Pruess, K. 2004. Numerical simulation of CO₂ disposal by mineral trapping in deep aquifers Applied Geochemistry, 2004, Vol. 19(6), pp. 917 – 936.



- Xu, T., J. A. Apps, and K. Pruess (2003), Reactive geochemical transport simulation to study mineral trapping for CO₂ disposal in deep arenaceous formations, *J. Geophys. Res.*, 108(B2), 2071.
- Xu, T., Kharaka, Y.K., Doughty, C., Freifeld, B.M. & Daley, T.M. 2010. Reactive transport modeling to study changes in water chemistry induced by CO₂ injection at the Frio-I Brine Pilot Chemical Geology, 2010, Vol. 271(3-4), pp. 153 – 164.
- Zerai, B., Saylor, B.Z. & Matisoff, G. 2006. Computer simulation of CO₂ trapped through mineral precipitation in the Rose Run Sandstone, Ohio Applied Geochemistry, 2006, Vol. 21(2), pp. 223 – 240.
- Zhang, W., Li, Y., Xu, T., Cheng, H., Zheng, Y. & Xiong, P. 2009. Long-term variations of CO₂ trapped in different mechanisms in deep saline formations: A case study of the Songliao Basin, China International Journal of Greenhouse Gas Control, 2009, Vol. 3(2), pp. 161 – 18.